Title: Long-term response and design of two geosynthetics: effect of field installation damage

Authors: M. Pinho-Lopes[*1], A.M. Paula[2] and M.L. Lopes[3]

[1] Lecturer, Faculty of Engineering and the Environment, University of Southampton, Highfield, Southampton SO17 1BJ, United Kingdom, Email: M.Pinho-Lopes@soton.ac.uk

[2] Assistant Professor, Department of Applied Mechanics, Polytechnic Institute of Bragança, Campus de Santa Apolónia, 5300-253 Bragança, Portugal, E-mail: mpaula@ipb.pt

[3] Full Professor, Department of Civil Engineering, Faculty of Engineering, University of Porto, Rua Dr. Roberto Frias, s/n 4200-465 Porto Portugal, E-mail: lcosta@fe.up.pt

[*] Corresponding author

Abstract:

This paper contributes to understanding how installation damage of geosynthetics influences their long-term response and design. A geotextile and a geogrid were exhumed after installation under real conditions; their long-term tensile behaviour was investigated using conventional creep and creep rupture tests. Reduction factors for installation damage, creep and their combined effect were computed. The main aim of the paper was to assess how the long-term response of the geosynthetics was influenced by installation damage and whether it would be necessary to update current design approaches. The installation damage affected the mechanical response of both geosynthetics; important strength reductions were observed, particularly for the most severe installation conditions. The results indicate that, contrary to what has been reported in the literature, the creep rupture response of the geotextile changed after installation damage. When tested under similar creep loads (fraction of the sample tensile strength), both geosynthetics exhibited reduced potential for creep rupture and smaller strains at the end of primary creep. Changes in stiffness were less important than those for strength, for both short- and long-term response. There was synergy between installation damage and creep; the traditional approach to design was unsafe for the geotextile and slightly conservative for the geogrid.

Keywords:

Geosynthetics, installation damage, tensile strength, creep, creep rupture, isochronous curves, reduction factors, synergy, stiffness

1 INTRODUCTION

Installation damage of geosynthetics is one of the most relevant aspects to consider for design of geosynthetic-soil structures, as it will affect their performance significantly. In each project, particularly for soil reinforcement applications, the effects of installation damage should be estimated using project-specific data or, when unavailable, using interpolations from data obtained under similar installation conditions.

The aim of this paper was to assess the influence of field installation damage on the long-term tensile behaviour of two geosynthetics and derive relevant design parameters. This enabled clarifying the level to which the long-term response of the geosynthetics was affected by installation damage. The installation damage was induced in the field under real conditions. The changes in the the short-term tensile response of the materials and their long-term response (creep behaviour and time to creep rupture) were assessed.

2 BACKGROUND

The design life of geosynthetic-soil structures varies and, in some cases, it can exceed 100 years. Thus, geosynthetics must be selected to ensure they maintain adequate values of relevant functional properties through their design life. The durability of geosynthetics is key for design and is influenced by installation damage (normally associated with mechanical damage), sustained load (static or dynamic), temperature, weathering and chemical degradation. This paper focuses on installation damage and sustained static loading.

Particularly for reinforcement applications, current practice requires estimating the long-term allowable strength of the reinforcements available at the end of the design life by determining separate reduction factors representing the strength loss expected due to different unrelated mechanisms (FHWA – Elias et al. 2001, BSI 2007b - EN ISO 20432; Greenwood et al. 2012, EBGeo 2012, AASHTO 2012). This approach can be used for both allowable stress design and limit states design (or load and resistance factor design), as described by Bathurst and Miyata (2015). In limit state design, maximum acceptable target probability of failure for relevant limit states have to be met. For that, it is necessary to calibrate relevant load and resistance factors using reliability theory and, thus, defining consistent and reasonable target probability of failure for relevant limit states. Examples of this approach and the calibration of relevant load and resistance factors have included installation damage (Bathurst et al. 2011, Miyata and Bathurst 2015), creep rupture (Bathurst et al. 2012), and installation damage and creep (Bathurst and Miyata 2015).

Equation 1 represents the allowable long-term strength of a geosynthetic reinforcement (T_{al}). The designations in BSI (2007b), EN ISO 20432, are adopted herein, where: T_{char} is a statistical value derived from the mean strength of the geosynthetic; RF_{CR} is the reduction factor for creep (sustained static load); RF_{ID} is the reduction factor for installation damage (or mechanical damage); RF_{W} is the reduction factor for weathering (during exposure before installation or of material permanently exposed); RF_{CH} is the reduction factor for chemical and biological effects (or the environment). Commonly, the characteristic strength of the geosynthetic reinforcement (T_{char}) corresponds to a 95% confidence interval or is obtained in the USA from the mean tensile strength value by subtracting two times the corresponding standard deviation.

$$T_{al} = \frac{T_{char}}{RF_{CR} \times RF_{ID} \times RF_{W} \times RF_{CH}} \quad (1)$$

For example for geosynthetic-reinforced soil structures, the short- and long-term tensile properties of geosynthetics play a fundamental role on the design, as many design methods aim to prevent tensile failure of the reinforcement due to excessive creep deformation, potentially accelerated by its degradation (Kongkitkul et al. 2007). According to Greenwood et al. (2012), installation damage and its consequences are relatively immediate (when considering the geosynthetic lifetime), with a rapid and irreversible reduction in strength with no further change with time. On the contrary, excluding any environmental or installation damage effects, the strength of geosynthetics under sustained load decreases over a relatively short period before failure (Greenwood et al. 2012). The influence of installation damage on the long-term response of geosynthetics has been studied by several authors, such as Wrigley (1987), Bush (1988), Allen and Bathurst (1996), Pinho-Lopes et al. (2001), Pinho-Lopes et al. 2002; Greenwood (2002), Paula et al. 2008; Cho et al. (2006), Jeon and Bouazza (2010), Bathurst and Miyata (2015). Many of these authors agree that the conventional approach to design, where reduction factors are considered independent, is generally conservative, resulting in safe design solutions. Due to several difficulties in long-term testing of samples submitted to installation damage, the conventional approach is the preferred one.

To check the validity of assumptions currently used for the design of geosynthetics, this paper focuses on obtaining design parameters for two geosynthetics exhumed after installation damage, for both ultimate and serviceability limit states. The synergy between installation damage and the creep of these geosynthetics is analysed and discussed.

3 EXPERIMENTAL PROGRAM

3.1 Test program

The test program consisted of characterising the short- and long-term tensile response of samples of two geosynthetics exhumed after field installation trials. The main aim of the present study was to assess if the long-term response of the field damaged geosynthetics could be estimated realistically from the short-term response of damaged samples. Isochronous curves, representing long-term force-strain relationships, were derived from the test results for both undamaged and exhumed samples. Sherby-Dorn plots were used to identify creep stages. The test program implemented was summarised in Table 1.

3.2 Geosynthetics

Two geosynthetics with different structure were studied (Figure 1). Geotextile GTX was formed by woven polypropylene (PP) tapes. GTX had 65kN/m of nominal tensile strength in the machine direction, nominal mass per unit area of 320g/m^2 and thickness of 1.2mm. Geogrid GGR was formed by high tenacity polyester (PET) yarns woven into a grid structure covered with black polymeric coating. The nominal tensile strength of GGR in the machine direction was 55kN/m. Geogrid GGR had openings of 18mm x 18mm and variable thickness (1.5mm for the ribs to 2.3mm for the junctions). The ribs were 4mm wide (machine direction) and 5mm wide (cross-machine direction).

3.3 Installation damage

Two sets of test beds were built (on two different road construction sites), each with a different backfill soil that was compacted to two different energies. Typical procedures for soil reinforcement applications were used and good practice solutions were adopted. These included: placing the geosynthetics on a layer free from roots and sharp materials; ensuring a minimum soil coverage of 0.15m to the geosynthetics before allowing construction traffic over them; limiting the maximum particle size in the initial lift to less than 1/4 of the lift thickness (as recommended by Richardson 1998).

The test beds (Figure 2) consisted of a compacted foundation layer (built over the road base), the layer of geosynthetics and two compacted soil lifts. The total height of the test bed was 0.60m, as each soil lift was 0.20m high, after compaction with a vibratory roller (operating weight of 153kN). A nuclear densymeter was used for monitoring the compaction degree. After completion of the test beds, the geosynthetics were exhumed in two stages: 1) using machinery;

2) manually. The construction equipment used to spread, level and compact the soil was the same in both sets of test beds, to allow for comparable conditions.

In each set of test beds, a different backfill soil was utilised: soil S1, a crushed aggregate; and soil S2, a residual soil from granite. The soils selected were available on the construction sites and tried to represent opposite scenarios: soil S1 was well-graded and is adopted often in road construction, while soil S2 was a local soil, which had to be reutilised for the road construction on that particular site to minimise earth movements. Some characteristics of soils S1 and S2 are summarised in Figure 3. More details can be found in: Pinho-Lopes and Lopes (2014), who analysed the influence of field installation damage on the tensile response of several other geosynthetics; Pinho-Lopes et al. (2015), who analysed the influence of installation damage on the pullout response of other geosynthetics; Pinho-Lopes et al. (2016), who studied the influence of installation damage on the soil-geosynthetic interaction for the two geosynthetics studied herein. Other authors have reported using comparable soils, such as Cho et al. (2006) and Jeon and Bouzza (2010) who used weathered granite soils and gravel.

The compaction energy was defined as that necessary to achieve the desired relative compaction of each soil, using the soil standard Proctor (ASTM D 698-00a) as a reference. The two compaction energies used, designated as CE1 and CE2, corresponded to a relative compaction of 90% and 98% of the soil standard Proctor, representing a poorly and a well compacted soil, respectively. The maximum dry unit weight, γ_{dmax}, and the optimum water content, w_{opt}, of the soils were (ASTM D 698-00a): for soil S1, γ_{dmax}=20.7kN/m^3 and w_{opt}=7.8%; and for soil S2, γ_{dmax}=18.8kN/m^3 and w_{opt}=11.3%.

Geotextile GTX was not installed in soil S2 with CE1 (Table 1), as some samples were stolen from the construction site where the test beds were built.

3.4 Characterisation of the geosynthetics

The geosynthetics were characterised using visual inspections of the different types of samples (undamaged and exhumed) particularly with a scanning electronic microscope (SEM), to better understand the type and the severity of the damage induced. Such observations may help understanding the influence of installation damage on the response of the geosynthetics measured from the tests.

Tensile tests were carried out using the procedures described in EN ISO 10319:2008 (BSI 2008), using hydraulic jaws and measuring strain with a video-extensometer. Each sample was characterised using five valid specimens. To study the long-term mechanical response

tensile creep and creep rupture tests (EN ISO 13431:1999, BSI (1999)) were used, testing a minimum of three specimens for each load level (per sample). It was necessary to increase the number of specimens for the damaged samples, due to the heterogeneity of responses observed. The specimens were 100mm wide (GTX) and ~105mm (5 bars) wide (GGR). The strains were measured using video-extensometers. All samples were tested in the machine direction.

Large rectangular samples of the geosynthetics (~25m^2 each) were installed in the test beds (Figure 2). To choose the specimens to be tested after exhumation, an objective geometric criterion was defined. For that purpose, within the large rectangles, distinctive areas were allocated to take specimens for the different types of characterisation tests used, by choosing similar positions on the samples.

4 RESULTS AND DISCUSSION

4.1 Visual inspection

The visual observation of undamaged and exhumed specimens allowed comparing their structures and the corresponding changes induced by the installation damage. Visual inspections were done using a high-resolution SEM (model JEOL JSM 6301F), with different magnifications (between 10 and 2000). Due to the accumulation of soil particles on their surface, the specimens had to be cleaned (avoiding additional damage). For both geosynthetics, the specimens were taken from similar positions within the samples. To ensure the specimens were representative of the corresponding sample, a global visual assessment of the damage induced was undertaken.

The SEM images clearly show the woven structure and the constituent tapes of GTX (Figure 4). The undamaged samples had some singularities, such as loose filaments. The tapes were not continuous and exhibited some openings. After installation damage, the overall aspect of the samples was changed. The sample installed in soil S2 and compacted to CE2 exhibited local abrasion, scratching and fibrillation of its tapes. The sample installed in soil S1 with CE2 was the most affected, with cuts, fibrillation, puncturing and increase of surface roughness. The surface changes observed were most pronounced after installation in soil S1 and CE2.

The yarns of GGR were distinguishable under its coating (Figure 5), particularly for the undamaged sample. Despite having been cleaned, the exhumed specimens exhibited soil particles on their surface. Soil S1 was the more aggressive soil for GGR: when compacted with CE1 there was partial removal of its coating; when compacted with CE2 GGR had significant fibre cuts, partial removal of the coating and fibre damage. After installation in soil S2, the

observed changes were: for compaction energy CE1, partial removal of coating, accumulation of soil particles and some damage on the coating (cracking and openings); for compaction energy CE2, removal of coating, exposing fibres, accumulation of soil particles and surface abrasion.

Contact with sharp-edged materials (such as stones) typically induces fibre cutting of geosynthetics (e.g., woven geotextiles, geogrids and strips). According to Watn and Chew (2002), a polymeric coating can reduce the susceptibility of geosynthetics for fibre cutting and the consequent tensile strength reductions. As discussed above, for GGR the coating was significantly damaged and, in some cases, not sufficient to protect the yarns from becoming exposed or being cut. Such exposure would likely lead to additional damage of the yarns and additional strength reductions during service of the geogrid (due to mechanical damage or other forms of degradation).

Observations indicated that soil S1 was more aggressive to GTX and GGR than soil S2. The differences observed were related to the particle angularity and size distributions of the soils. Soil S1 was formed by large, crushed, thus angular, particles, while soil S2 was a residual soil from granite, with rounder and smaller particles (previously submitted to geological weathering and aging processes). These observations were in good agreement with what was discussed by Greenwood et al. (2012).

4.2 Short-term tensile properties

The short-term tensile properties measured were summarised in Table 2. These included the mean values (for 5 specimens) of the maximum tensile strength (T_{max}, kN/m), the corresponding strain (ε_f, %) and the secant tensile stiffness modulus at 2% and 5% strain (respectively, $J_{2\%}$ and $J_{5\%}$, kN/m), as well as the 95% confidence intervals for all quantities. The 100(1-α) percent confidence interval for the population mean, $\bar{x}$, was given by Equation 2 (σ, standard deviation; n, size of the sample; α, level of significance, taken as 0.05, for a 95% confidence interval (CI); $t_{1-\left(\frac{\alpha}{2}\right)}$, t-Student distribution). The variables studied were assumed normally distributed and, therefore, the confidence intervals for the corresponding means could be determined using the t-Student distribution (Zar, 2009). This approach used to estimate the 95% confidence values is less severe than using two times the standard deviation. As it takes into account the size of the sample and its standard deviation, the approach used is likely to be more realistic than using two times the standard deviation (provided the variables are normally distributed).

$$CI = t_{1-\left(\frac{\alpha}{2}\right)} \frac{\sigma}{\sqrt{n}} \quad (2)$$

After installation damage all properties analysed were reduced (except $J_{2\%}$ for GTX ID S2 CE2), although with different magnitudes. The tensile strength was the most affected property, with reductions ranging between 9.1% (for GTX ID S2 CE2) and 66% (for GTX ID S1 CE2). The property least affected by installation damage was the secant stiffness $J_{2\%}$ for GTX and $J_{5\%}$ for GGR. Bush (1988) reported similar results for HDPE geogrids. For woven materials and uniaxial geogrid products, the stiffness can quantify the resistance to installation damage under real conditions better than the tensile strength (Allen and Bathurst 1994). The stiffness values of GTX and GGR were usually less affected by the installation damage induced than their tensile strength, with variations ranging between: $J_{2\%}$, +1.3% (GTX ID S2 CE2) to -29.4% (GGR ID S1 CE2); $J_{5\%}$, -2.2% (GTX ID S2 CE2) to -27.6% (GTX ID S1 CE2).

GTX had a small thickness (1.2mm) and most of its tapes had several contact points with the adjacent aggregate during construction of the test beds. The woven structure of GTX also had an important role on the tensile response observed after installation: for increasing strains, a localised damage will likely propagate over a significant area. The SEM observations showed that in some cases the tapes were significantly affected by installation, which led to a reduced resistant section (due to cuts, tape fibrillation and/or abrasion). Additionally, the puncturing and fibre / tape cutting observed created fragility points, not able to withstand or transmit loads during the tensile test. Thus, the loads applied during the tensile tests had to arch around damaged areas, generating stress concentration on adjacent sections of the specimens, which in turn provoked premature failure. For low loads (such as those for 2% strain) the effect described was not as important, which indicates that the load-strain response of GTX under service loading may not be as affected by installation damage as the tensile strength was in the tests.

GGR exhibited a similar response to damage, due to its woven structure; however, an overall better behaviour was observed, as during the field installation trials the contact area with the surrounding soil was smaller than that of GTX. The SEM observations of GGR seem to indicate that installation affected mostly the coating (though fibre cutting was particularly relevant after ID S1 CE2). Therefore, although the coating was often removed due to installation, it was able to protect the fibres to a certain degree, ensuring that the load bearing elements (partially) survived the damage.

Additionally, the trend identified from the SEM images was confirmed by the tensile tests results: soil S1 was more aggressive to the geosynthetics studied than soil S2, due to the different particle sizes and angularity.

After installation damage the 95% confidence interval for the tensile strength of GGR was larger than the corresponding value for the undamaged material. For GTX two exceptions to this trend were found (after ID S1 CE2 and ID S2 CE2). However, as the mean values for the tensile strength of all samples tested decreased after exhumation, analysing the values of the confidence intervals normalised to the corresponding mean value was found more appropriate. Such values indicate that after damage the scatter of the tensile strength increased for all samples of GGR and GTX (except GTX ID S2 CE2).

4.3 Long-term tensile properties

4.3.1 Creep rupture tests

The creep rupture test results were summarised in Figures 6 and 7, respectively, for GTX and GGR. These figures include the creep rupture curves (linear approximations in a semi-logarithmic scale), the corresponding equations and coefficients of determination (R^2), and the lower confidence limit curves for 95% (designated as LCL 95%), as defined in ISO/TR 20432 (BSI, 2007b). Figures 6a and 7a refer to the time to rupture of the different samples analysed as a function of $RS_{CRsample,und}$ (Equation 3), the retained strength of the different samples of geosynthetic studied relatively to the undamaged sample (with tensile strength $\bar{T}_{TTund}$). Figures 6b and 7b include the same data as a function of $RS_{CRsample,sample}$ (Equation 4), the retained strength of each sample. In the latter, the creep rupture load applied to the specimen, $T_{CRsample}$, was normalised to the tensile strength of each sample ($\bar{T}_{TTsample}$) obtained from the tensile tests (Table 2): $\bar{T}_{TTund}$ for the undamaged sample and the corresponding $\bar{T}_{TTdam}$ for each damaged sample.

$$RS_{CRsample,und} = \frac{T_{CRsample}}{\bar{T}_{TTund}} \quad (3)$$

$$RS_{CRsample,sample} = \frac{T_{CRsample}}{\bar{T}_{TTsample}} \quad (4)$$

The creep rupture curves of the undamaged samples showed little scatter (R^2~0.94) that tended to increase after installation damage (ranging between R^2=0.53 (GGR ID S1 CE1) and R^2=0.90 (GGR ID S2 CE2)). To address the dispersion of responses observed, for some damaged samples a higher number of specimens was tested. Many specimens of GTX installed in soil S1 CE2 (which had the highest tensile strength reduction after exhumation, 66%)

exhibited a fragile response, with ruptures occurring less than 1 minute after the load application, due to the rapid propagation of damage through the woven structure.

Although apparently both geosynthetics have a reduced creep rupture resistance after installation damage (Figures 6a and 7a), GTX and GGR exhibited a different creep rupture response after installation damage (Figures 6b and 7b). For GGR, the creep rupture curves for the retained strength of each sample, $RS_{CRsample,sample}$, are very close (Figure 7b); the main differences were observed for samples exhumed from soil S2 (change in slope of the creep rupture curves between 12% and 17%). For GTX, the creep rupture curves for $RS_{CRsample,sample}$ (Figure 6b) exhibited reduced slope after installation damage (variations ranging between 37% and 101%). For the most severely damaged sample (GTX ID S1 CE2), the zero intersect of the corresponding creep rupture curve was also significantly changed (reduced 27%). These results indicate that the creep rupture strength of exhumed GGR can be estimated from the creep rupture response of the undamaged GGR for a comparable loading period, while for GTX such procedure may lead to an unsafe creep rupture strength prediction. This response is contrary to what has been reported by other authors. The different responses observed are likely to be linked to the different constituent polymers (as discussed in section 4.3.2) and structures of these geosynthetics.

4.3.2 Creep tests

The creep tests were performed for load levels, relatively to the undamaged material, between 68% and 7% (Figure 8a and 9a), which correspond to 73% to 20% of the samples' tensile strength (Figure 8b and 9b); many tests were stopped after 1440 hours (~two months), without rupture. As expected, higher load levels applied to the geosynthetics led to higher strains, for both reference (undamaged) and damaged samples.

GTX (Figure 8) exhibited a typical response of a polyolefin material, with an initial stage of primary creep (linear creep in a semi-log scale). The tertiary creep, characterised by an increase of the strain rate leading to failure, is visible for most samples that ruptured (undamaged and exhumed after installation damage). Particularly for the most severe installation conditions (ID S1 CE2), the kink in the creep curves was visible also for lower load levels (compared to the undamaged sample, Figure 8a), indicating earlier failure. After installation damage, the scatter of results generally increased, particularly for the sample exhumed from S1 CE1. When comparing the creep response of each sample of GRX (Figure 8b), the results indicate that after installation damage tertiary creep is likely to occur for lower strains relatively to the undamaged sample.

For GGR (Figure 9), most creep curves showed linear creep strains in a semi-log scale, typical of a PET product. The failures observed were not always preceded by a rapid increase of the strain rate. Therefore, for this material, anticipating failure was more difficult than for GTX. When submitted to similar load levels relatively the samples' tensile strength (Figure 9b), the installation damage induced caused earlier failures of GGR, especially after the most severe installation conditions.

Sherby-Dorn plots, representing $\log\left(\frac{d\varepsilon}{dt}\right)$ versus strain, ε (where $\frac{d\varepsilon}{dt}$ is the strain rate), for specimens tested under similar load levels, were generated to analyse if the installation damage induced affected the creep stages of GTX and GGR. Figures 10 and 11, respectively, illustrate results for specimens of GTX and GGR submitted to similar creep loads represented as a fraction of both the tensile strength of the undamaged sample, $\bar{T}_{TTund}$ (Figures 10a and 11a) and the tensile strength of each sample, $\bar{T}_{TTsample}$ (Figure 10b and 11b).

The Sherby-Dorn curves for specimens that did not rupture are concave upward or exhibit an outward sweep, which indicates that secondary or tertiary creep is occurring or has the potential for developing and that rupture is likely (WSDOT 2009). This trend is particularly visible for GTX (Figure 10), but also for GGR (Figure 11). For specimens tested under the same load level, the position of the curves within the Sherby-Dorn plots can indicate their potential for creep rupture, as curves with higher creep strain rates developing for higher strains (thus, closer to the upper right left corner of the plot) indicate that creep rupture is more likely to occur (WSDOT 2009). From Figures 10a and 11a, and with the exception of the higher load level considered (60% of $\bar{T}_{TTund}$ for both GTX and GGR), the potential for creep rupture of both geosynthetics increased after installation damage. However, when analysing the response of GTX and GGR for specimens tested for the same load relatively to $\bar{T}_{TTsample}$ (Figures 10b and 11b), all exhumed specimens have a reduced potential for creep rupture compared to their corresponding undamaged specimen tested under the same creep load.

To identify the transition between creep stages, the derivate of the Sherby-Dorn curves ($\frac{d}{d\varepsilon}\left[\log\left(\frac{d\varepsilon}{dt}\right)\right]$, representing the slope of the Sherby-Dorn plots) were calculated. When that slope is 0, there is a transition from primary creep (negative slope) to tertiary creep (positive slope). The transition can be sudden, for specimens not exhibiting secondary creep, or it can include a steady-state creep rate represented by several points with zero derivate (secondary creep). Thus, herein, the strain at the beginning of secondary creep or tertiary creep (for specimens not exhibiting secondary creep) was approximated as the strain for $\frac{d}{d\varepsilon}\left[\log\left(\frac{d\varepsilon}{dt}\right)\right] =$

0. Figure 12 represents the strain for which $\frac{d}{d\varepsilon}\left[\log\left(\frac{d\varepsilon}{dt}\right)\right] = 0$ for specimens tested under the same creep load relatively to $\bar{T}_{TTund}$ and $\bar{T}_{TTsample}$, for GTX and GGR.

When analysing the data plotted as a function of $\bar{T}_{TTund}$, the trends exhibited by GTX and GGR seem different: for each creep load after installation damage GTX exhibited an increase in the strain at the beginning of secondary or tertiary creep (Figure 12a); for GGR there was no significant change (Figure 12b). However, analysing the creep response of the different samples of two geosynthetics plotted as a function of $\bar{T}_{TTsample}$, the trend observed was quite different – for each creep load there was a reduction of the strain at the beginning of secondary or tertiary creep for all samples of GGR (Figure 12d) and all samples of GRX (Figure 12c), except ID S2 CE2 (where $\bar{T}_{TTsample} \cong 0.75 \times \bar{T}_{TTund}$). This reduction was more important for more severe damage conditions (for which test results are available) for both GTX (ID S1 CE2) and GGR (ID S1 CE1). This seems to indicate that the installation damage induced in these two geosynthetics influenced their creep response and that after exhumation the strain for the creep stage transition was anticipated, i.e., occurred for smaller strains.

4.4 Isochronous load-strain curves

Figure 13 summarises the load-strain responses for specific instants for samples undamaged and submitted to field installation. The curves for 1 minute were similar to the corresponding tensile tests curves (t=0); the differences observed can be attributed to the different test procedures.

GTX (undamaged and exhumed after installation) exhibited reductions in stiffness, evident after t=24 hour, and in tensile strength. GGR exhibited reductions in stiffness and in strength with time; however, these are less important. These differences were most likely due to the different constituent polymers of the geosynthetics and their different structure. The influence of the installation damage induced on the isochronous curves seemed to be analogous for all types of damaged samples analysed. The isochronous curves of GGR for t=0 exhibited a typical S-shape for low strains (as described by Liu and Ling 2007 for PET geogrids). However, due to the load levels applied and strains measured, that shape could not be captured for other curves. Thus, the secant stiffness of GGR for 2% strain is not discussed herein.

Figure 14 illustrates the changes in stiffness for 2% and 5% strain with time obtained from the isochronous curves, represented by $J_{2\%}$ and $J_{5\%}$. For GTX, the secant modulus of stiffness decreased with time. For t > 1 hour, the stiffness curves for undamaged and exhumed samples are approximately parallel, indicating that the long-term reduction of stiffness after

installation could be estimated using the long-term response of the undamaged sample. This is discussed further in section 4.5.2. For GGR, only data for $J_{5\%}$ is presented. After installation in S1 CE1 and S2 CE1, the values for $J_{5\%}$ are very close to that of the undamaged sample, however, the data from the tensile tests does not follow the same trend. For the sample submitted to ID S1 CE2, there was a reduction in stiffness for all the data points; the corresponding curve is roughly parallel to that of the undamaged sample. For the sample ID S2 CE2, there is a mixed response: while for shorter times the reduction in stiffness is relatively small, for longer times ($t \geq 10000$ hour) the stiffness is quite close to that of the undamaged sample.

For design, the mechanical properties of geosynthetics at the end of their lifetime should be quantified. Although most design codes use a tensile strength, the secant stiffness modulus or the tensile force for a specific strain of some types of products can better represent their mechanical response. The isochronous curves could be used for the design of geosynthetics, as they represent the load-strain response of the material for a defined instant, provided relevant / adequate reduction factors are applied. In this paper, these curves represent such response more realistically, as they allow for the installation damage effects. Nevertheless, additional relevant mechanisms affecting the long-term strength, stiffness and strain of the materials may need to be considered in design.

Using the data from the isochronous curves (Figure 13) and the information on Figure 14, the stiffness values for GTX and GGR ($J_{2\%}$ and $J_{5\%}$) after 30 years were estimated. The data in Figure 14 was fitted using statistical regression analyses; as for the creep rupture data, the independent variable was plotted on the y-axis and the dependent variable on the x-axis (ISO/TR 20432 (BSI, 2007b)). Such data was then used to estimate relevant reduction factors (section 4.5.2).

4.5 Reduction factors

Using the test results, several reduction factors were determined. The aim was to compare the influence on some of the properties analysed (T, $J_{2\%}$ and $J_{5\%}$) of installation damage, creep (sustained loading, for a design life t_D) and their combined effect. Reduction factors for installation damage and creep were summarised in Table 3, for t_D=30years.

4.5.1 Installation damage (short-term response)

Reduction factors for installation damage were determined from the tensile tests results using the traditional formulation, i.e. measured tensile strength ($RF_{ID\ (T)}$), and using the measured secant stiffness values for strains of 2% ($RF_{ID\ (J2\%)}$) and 5% ($RF_{ID\ (J5\%)}$) (Table 3, columns [1]

to [3]). These reduction factors were calculated as the ratio between mean values of the relevant property (X) for the undamaged samples, $\bar{X}_{und}$, and that after installation damage, $\bar{X}_{dam}$ (Equation 5). The minimum acceptable value for all reduction factors is 1.0. Usually, the reduction factor $RF_{ID\,(T)}$ is used in Equation 1 as RF_{ID}.

$$RF_{ID\,(X)} = \frac{\bar{X}_{und}}{\bar{X}_{dam}} \tag{5}$$

The reduction factor $RF_{ID\,(T)}$ ranged from 1.10 (GTX ID S2 CE2) to 2.94 (GTX ID S1 CE2 - the most severe installation conditions). The reductions factors $RF_{ID\,(J2\%)}$ or $RF_{ID\,(J5\%)}$ obtained from the stiffness data (tensile tests) are less conservative, and are likely to be more representative of the resistance to installation damage for woven materials and uniaxial geogrids, as reported by Allen and Bathurst (1994).

4.5.2 Creep and creep rupture (long-term response)

The creep reduction factor for the tensile strength ($RF_{CR\,(T)}$) for the different samples studied was determined using the data from Figures 6b and 7b, to isolate the influence of creep on the response of each sample. For a design time t_D, the creep reduction factor for creep was determined as the inverse of the retained strength of each sample at $t=t_D$, $RS_{CRsample,sample\,(t=tD)}$, using Equation 6. The reduction factor $RF_{CR\,(T)}$ obtained from the data for the undamaged sample is normally used in Equation 1 as RF_{CR}.

$$RF_{CR\,(T)} = \frac{\bar{T}_{TTsample}}{T_{CRsample\,(t=t_D)}} = \frac{1}{RS_{CRsample,sample\,(t=t_D)}} \tag{6}$$

For the undamaged samples and t_D=30 years, $RF_{CR\,(T)}$ was 2.08 for GTX and 1.68 for GGR (Table 3, column [4]). The values of $RF_{CR\,(T)}$ for the damaged samples (Table 3, column [4]) illustrate the different influence of installation damage on the creep rupture response of GTX and GGR. For GTX, the predictions of the creep rupture response after damage using the results for the undamaged sample seem to be unsafe, while the creep rupture response of GGR was not significantly changed. The results for GTX show that, for the installation conditions considered, such installation has changed the creep rupture response of GTX.

As for the tensile tests data, creep reduction factors for the secant stiffness ($RF_{CR\,(J2\%)}$ and $RF_{CR\,(J5\%)}$) were determined for both undamaged and damaged samples using Equation 7 (Table 3, columns [7] and [8]). This equation represents the ratio between the mean value of the secant stiffness of a sample obtained from the tensile tests, $\bar{J}_{TTsample}$ (Table 2), and the corresponding long-term secant stiffness ($J_{2\%}$ or $J_{5\%}$) extrapolated from the isochronous curves for $t=t_D$ ($J_{CRsample\,(t=tD)}$).

$$RF_{CR\,(J)} = \frac{\bar{J}_{TTsample}}{J_{CR\ sample\ (t=t_D)}} \quad (7)$$

These factors represent the influence of creep (sustained static loading) on the stiffness for 2% and 5% strain of the geosynthetics. The values obtained for the undamaged samples were: $RF_{CR\,(J2\%)}$=2.96 and $RF_{CR\,(J5\%)}$=4.04, for GTX; $RF_{CR\,(J5\%)}$=1.04, for GGR. Analysing the corresponding values for the damaged samples (Table 3, columns [7] and [8]), it seems that after installation damage the influence of creep on $J_{2\%}$ and $J_{5\%}$ was reduced, particularly for GTX. In fact, the reduction factors for the secant stiffness of the damaged samples are smaller than those for the corresponding intact sample.

The reduction factors for the secant stiffness obtained from the tensile tests data (Table 3, columns [2] and [3]) were also compared to those obtained from the isochrones curves data (Table 3, columns [7] and [8]). For GTX, the tensile tests data underestimates the long-term reduction in stiffness observed after installation, except for $J_{5\%}$ after ID S1 CE2, the most severe installation conditions. For GGR, only data for $J_{5\%}$ can be compared. In this case, for the samples compacted to CE2, the tensile tests underestimate the reduction in stiffness predicted using the isochronous curves.

4.5.3 Installation damage and creep and creep rupture

The reduction factors for the combined effect of installation damage and creep on the tensile strength, $RF_{ID+CR\,(T)}$, were determined using Equation 8, as the ratio between the tensile strength of the undamaged sample ($\bar{T}_{TTund}$) and the creep rupture load of the damaged sample for $t=t_D$ ($T_{CR\ sample(t=t_D)}$). These values (Table 3, column [5]) are also the inverse of the retained strength of the different samples of geosynthetic exhumed, relatively to the undamaged sample, for $t=t_D$. $RF_{ID+CR\,(T)}$ allows for synergy between installation damage and creep and can be used in Equation 1 instead of RF_{CR} x RF_{ID}.

$$RF_{ID+CR\,(T)} = \frac{\bar{T}_{TTund}}{T_{CR\ sample(t=t_D)}} = \frac{1}{RS_{CRsample,und\ (t=t_D)}} \quad (8)$$

The traditional approach, which assumes that installation damage and creep are independent, was applied, multiplying the corresponding reduction factors RF_{ID} x $RF_{CR\,(T)}$. The reduction factor for installation damage $RF_{ID\,(T)}$ was obtained from tensile tests (Table 3, column [1]) and RF_{CR} refers to the values from Equation 6 for the undamaged samples (Table 3, column [4]), 2.08 for GTX and 1.68 for GGR. The traditional approach (RF_{ID} x $RF_{CR\,(T)}$, Table 3, column [6]) led to unsafe estimates compared to the synergetic effect ($RF_{ID+CR\,(T)}$,

Table 3, column [5]), more importantly for GTX. For GGR, in general, the traditional approach gave a good estimate of the response of the damaged samples.

Similarly, these two approaches were used for the stiffness $J_{2\%}$ and $J_{5\%}$: traditional approach (Table 3, columns [10] and [12]) and allowing for synergy (Table 3, columns [9] and [11]). For GTX, the traditional approach lead to unsafe estimates of all properties analysed (T, $J_{2\%}$ and $J_{5\%}$), except for $J_{5\%}$ for GTX ID S1 CE2. For GGR, while for T synergy did not affect the results significantly, for $J_{5\%}$ the traditional approach was found conservative (after installation in both soils compacted to the lower compaction energy, ID S1 CE1 and ID S2 CE1) and unsafe (for the higher compaction energy, ID S1 CE2 and ID S2 CE1).

5 CONCLUSIONS

In this paper, the long-term tensile behaviour of two geosynthetics exhumed after field installation damage was investigated. The analysis was complemented by examining changes in their short-term mechanical response and by performing visual inspections of the samples (using scanning electron microscope images). Reduction factors for installation damage, creep and their combined effect for different scenarios were presented and discussed, thereby enlarging existing databases. The main aim was to assess if the long-term response of the geosynthetics was influenced by installation damage and, if that was the case, whether it would be necessary to update current design approaches.

The long-term mechanical response of the two geosynthetics was analysed relative to the strength of each sample, rather than to the corresponding undamaged sample (usual approach). This enabled isolating the long-term response (creep and creep rupture) of the undamaged and exhumed geosynthetics for direct comparison.

From the results the main conclusions are:

- The short-term response of the two geosynthetics was affected by installation damage, particularly for the geotextile and for the most severe conditions considered. The changes in mechanical response observed are related to the visual changes observed.
- The changes in stiffness observed were less important than the corresponding changes in strength, for both short- and long-term mechanical response. When reinforcement geosynthetics are placed in soil, their strains are often limited, preventing different failure mechanisms from occurring. Therefore, in most cases, changes in stiffness (obtained from tensile tests) could be used to represent the response of the geosynthetics for limit states that do not involve tensile failure of the geosynthetics.

- After installation damage the potential for creep rupture decreased when the specimens were submitted to similar load levels relative to the tensile strength of each sample (rather than to a similar load level relative to that of the undamaged sample). After installation damage the additional strain during the creep stage transition (end of primary creep) was anticipated.
- There was synergy between installation damage and creep: positive for GTX, as the traditional approach assuming independence was unsafe, negative for GGR, representing a slightly conservative design (negative synergy).
- The results for GGR indicate that current design approaches are adequate for that material. In contrast, the long-term response of the GTX was influenced significantly by installation damage and exhibited a different trend. Extrapolating the long-term response of GTX after installation damage, particularly the creep rupture strength for a given design life, from the long-term results of the undamaged sample led to optimistic long-term estimates of available tensile strength.

As the creep behaviour of geosynthetics may lead to creep failure of geosynthetic-reinforced structures, it is essential to estimate realistically the influence of installation damage on the creep and creep rupture response of geosynthetics. The results for GTX indicate a trend different from those reported previously in the literature and that current design approaches could be unsafe for this material under the installation conditions considered in this paper.

NOTATION

Basic SI units are given in parentheses.

$\frac{d\varepsilon}{dt}$	Strain rate (-)
$\frac{d}{d\varepsilon}\left[\log\left(\frac{d\varepsilon}{dt}\right)\right]$	Derivate of the slope of the Sherby-Dorn plots, $\log\left(\frac{d\varepsilon}{dt}\right)$-ε (-)
$J_{2\%}$	Secant tensile stiffness modulus at 2% of strain (N/m)
$J_{5\%}$	Secant tensile stiffness modulus at 5% of strain (N/m)
$\bar{J}_{TTsample}$	Mean value of the secant stiffness of a sample obtained from the tensile tests (N/m)
$J_{CR\ sample\ (t=t_D)}$	Long-term secant stiffness extrapolated from the isochronous curves for $t=t_D$ (n/m)
n	Size of sample (-)
R^2	Coefficient of determination (-)
RF_{CH}	Reduction factor for chemical and biological effects (or the environment) (-)
RF_{CR}	Reduction factor for creep (sustained static load) (-)
$RF_{CR\ (J)}$	Reduction factor for creep (sustained static load) for the secant stiffness (-)

$RF_{CR\ (T)}$	Reduction factor for creep (sustained static load) for the tensile strength (-)
RF_{ID}	Reduction factor for installation damage (-)
$RF_{ID+CR\ (J2\%)}$	Reduction factor for combined effect of installation damage and creep rupture obtained from the secant stiffness value for 2% strain (-)
$RF_{ID+CR\ (J5\%)}$	Reduction factor for combined effect of installation damage and creep rupture obtained from the secant stiffness value for 5% strain (-)
$RF_{ID+CR\ (T)}$	Reduction factor for combined effect of installation damage and creep rupture obtained from the tensile strength (-)
$RF_{ID\ (J2\%)}$	Reduction factor for installation damage obtained from the secant stiffness value for 2% strain (-)
$RF_{ID\ (J5\%)}$	Reduction factor for installation damage obtained from the secant stiffness value for 5% strain (-)
$RF_{ID\ (T)}$	Reduction factor for installation damage obtained from the tensile strength value (-)
$RF_{ID\ (X)}$	Reduction factor for installation damage obtained from the property X value (-)
RF_W	reduction factor for weathering (-)
$RS_{CRsample,sample}$	Retained strength under creep (sustained static load) relatively to the tensile strength of the sample (%)
$RS_{CRsample,sample\ (t=tD)}$	Retained strength under creep (sustained static load) relatively to the tensile strength of the sample at the design life t_D (%)
$RS_{CRsample,und}$	Retained strength under creep (sustained static load) relatively to the tensile strength of the undamaged sample (%)
$RS_{CRsample,und\ (t=tD)}$	Retained strength under creep (sustained static load) relatively to the tensile strength of the undamaged sample at the design life t_D (%)
t	Time (s)
$t_{1-\left(\frac{\alpha}{2}\right)}$	t-Student distribution for a level of significance α (-)
t_D	Design life of the geosynthetic reinforcement (s)
T	Tensile strength (N/m)
T_{al}	Allowable long-term strength of a geosynthetic (N/m)
T_{char}	Value derived from the mean strength of the geosynthetic (N/m)
$T_{CRsample}$	Creep rupture load of specimen from a sample (N/m)
$T_{CRsample\ (t=t_D)}$	Creep rupture load of specimen from a sample at the design life t_D (N/m)
T_{max}	Maximum tensile strength (N/m)
$\bar{T}_{TTdam}$	Tensile strength of a damaged sample (N/m)
$\bar{T}_{TTsample}$	Tensile strength of a sample (N/m)
$\bar{T}_{TTund}$	Tensile strength of the undamaged sample (N/m)
w_{opt}	Optimum water content (%)
$\bar{x}$	Population mean (*the same as the variable*)
$\bar{X}_{dam}$	Mean value of property X for the damaged material
$\bar{X}_{und}$	Mean value of property X for the undamaged material
α	Level of significance (-)
γ_{dmax}	Maximum dry density (N/m^3)
ε_f	Strain at break (%)
σ	Standard deviation (*the same as the variable*)

ABBREVIATIONS

CE Compaction energy

CI	Confidence interval
GTX	Geotextile
GGR	Geogrid
HDPE	High density polyethylene
ID	Installation damage
LCL	Lower confidence limit
PET	Polyester
PP	Polypropylene
S	Soil
SEM	Scanning electronic microscope

ACKNOWLEDGEMENTS

The authors would like to thank the financial support of FCT, Research Project PTDC/ECM/099087/2008 and COMPETE, Research Project FCOMP-01-0124-FEDER-009724.

REFERENCES

Allen, T. M. & Bathurst, R. J. (1994). Characterization of geosynthetic load-strain behavior after installation damage. Geosynthetics International, 1, No. 2, 181–199.

Allen TM and Bathurst RJ (1996) Combined allowable strength reduction factor for geosynthetic creep and installation damage. Geosynthetics International 3(3): 407–439.

AASHTO (2012) LRFD Bridge Design Specifications. American Association of State Highway and Transportation Officials. Washington, DC; USA.

ASTM (2000) D698-00a: Standard Test Methods for Laboratory Compaction Characteristics of Soil Using Standard Effort (12,400 ft-lbf/ft^3 (600 kN-m/m^3)). ASTM International, West Conshohocken, PA, USA.

Bathurst, R.J., Huang, B. and Allen, T.M. (2011) Analysis of installation damage tests for LRFD calibration of reinforced soil structures. Geotextiles and Geomembranes, 29 (3), 323-334.

Bathurst, R.J., Huang, B.Q. and Allen, T.M. (2012) Interpretation of laboratory creep testing for reliability-based analysis and load and resistance factor design (LRFD) calibration. Geosynthetics International, 19 (1), 39-53.

Bathurst, R.J. and Miyata, Y. (2015) Reliability-based analysis of combined installation damage and creep for the tensile rupture limit state of geogrid reinforcement in Japan. Soils and Foundations, 55 (2), 437–446.

BSI (1999) EN ISO 13431 (1999). Geotextiles and geotextile-related products — Determination of tensile creep and creep rupture behaviour. BSI, London, UK.

544 BSI (2008) EN ISO 10319 (2008). Geosynthetics. Wide-width tensile test. BSI, London, UK.
545 BSI (2007b) PD ISO/TR 20432 (2007). Guidelines to the determination of long-term strength
546 of geosynthetics for soil reinforcement. BSI, London, UK.
547 Bush, D.I. (1988) Evaluation of the effects of construction activities on the physical properties
548 of polymeric soil reinforcing elements. Proceedings of the International Symposium on
549 Theory and Practice of Earth Reinforcement, Fukuoka, Kyushu, Japan, 5-7 October 1988,
550 Balkema, Rotterdam, pp. 63-68.
551 Cho, S.D., Lee, K.W., Cazzuffi, D.A. and Jeon, H.Y. (2006) Evaluation of combination effects
552 of installation damage and creep behavior on long-term design strength of geogrids. Polymer
553 Testing, 25 (6), 819-828.
554 EBGEO (2012). Recommendations for Design and Analysis of Earth Structures using
555 Geosynthetic Reinforcements - EBGEO: Ernst & Sohn.
556 Elias, V., Christopher, B.R. and Berg, R.R. (2001) Mechanically stabilized earth walls and
557 reinforced soil slopes design and construction guidelines. Federal Highway Administration
558 (FHWA), NHI Course No. 132042, FHWA-NHI-00-043, Washington DC, USA, 394p.
559 Greenwood, J.H. (2002) The effect of installation damage on the long-term design strength of
560 a reinforcing geosynthetic. Geosynthetics International, 9 (3), 247-258.
561 Greenwood, J. H., Schroeder, H. F. & Voskamp, W. (2012). Durability of Geosynthetics, CUR
562 Building & Infrastructure, Gouda, the Netherlands, Publication 243.
563 Jeon, H.-Y. and Bouazza, A. (2010) Experimental investigation of installation damage for
564 geogrids. Proceedings of the Institution of Civil Engineers - Ground Improvement, 163 (4),
565 197-205.
566 Kongkitkul W, Hirakawa D and Tatsuoka F (2007) Creep rupture curve for simultaneous creep
567 deformation and degradation of geosynthetic reinforcement. Geosynthetics International,
568 14(4), 189-200.
569 Liu H and Ling HI (2007) Unified Elastoplastic-Viscoplastic Bounding Surface Model of
570 Geosynthetics and Its Applications to Geosynthetic Reinforced Soil-Retaining Wall
571 Analysis. Journal of Engineering Mechanics 133(7): 801-815.
572 Miyata, Y. and Bathurst, R.J. (2015) Reliability analysis of geogrid installation damage test
573 data in Japan. Soils and Foundations, 55 (2), 393-403.
574 Paula AM, Pinho-Lopes M, Lopes ML (2008) Combined effect of damage during installation
575 and long-term mechanical behaviour of geosynthetics. paper 185, theme 3 (Durability and
576 long term performance) of the 4th European Geosynthetics Conference, abstract book pp.
577 39, CD-ROM, 8p., Edinburgh, UK.

578 Pinho-Lopes M, Lopes ML (2014) Tensile properties of geosynthetics after installation damage.
579 Environmental Geotechnics 1(3), 161-178.
580 Pinho-Lopes, M., Lopes, M.L., Recker, C. and Muller-Rocholz, J. (2001) Analysis of the
581 combined effect of installation damage and creep of geosynthetics. International Conference
582 Composites in Construction (CCC2001), Porto, Portugal, 10-12 October, 2001. Leiden: A a
583 Balkema Publishers, pp. 379-384.
584 Pinho-Lopes M, Recker C, Lopes ML, Müller-Rochholz J (2002) Experimental analysis of the
585 combined effect of installation damage and creep of geosynthetics – new results. Proc. of
586 the 7th Int. Conf. on Geosynthetics, Vol. 4, pp. 1539-1544, Nice, France.
587 Pinho-Lopes M, Paula AM and Lopes ML (2015) Pull-out response of geogrids after
588 installation. Geosynthetics International, 22(5), 339-354.
589 Pinho-Lopes M, Paula AM and Lopes ML (2016) Soil–geosynthetic interaction in pullout and
590 inclined-plane shear for two geosynthetics exhumed after installation damage. Geosynthetics
591 International, 23(5), 331-347.
592 Richardson GN (1998) Field evaluation of geosynthetic survivability in aggregate road base.
593 Geotechnical Fabrics Report, September 1998, 34-38.
594 Watn A and Chew SH (2002) Geosynthetic damage – from laboratory to field, Keynote Lecture,
595 In *Proceedings of the 7th International Conference on Geosynthetics*, Nice, France, vol. 4,
596 pp. 1203-1226.
597 Wrigley N.E. (1987) Durability and long-term performance of Tensar polymer grids for soil
598 reinforcement. Materials Science and Technology, 3(3), 161-170.
599 WSDOT (2009). T 925 Standard Practice for Determination of Long-Term Strength for
600 Geosynthetic Reinforcement. Washington State Department of Transportation.
601 Zar JH (2009) Biostatistical Analysis, 5th ed. Harlow: Pearson Education, Upper Saddle River,
602 NJ, USA.

603 **TABLES**

604 **Table 1 - Test program implemented.**

Geosynthetic	Sample	SEM (Scanning Electronic Microscope) observations	Tensile tests EN ISO 10319	Creep and creep-rupture tests EN ISO 13431
GTX	UND	√	√	√ / *
	ID S1 CE1	√	√	√
	ID S1 CE2	√	√	√ / *
	ID S2 CE2	√	√	√ / *
GGR	UND	√	√	√ / *
	ID S1 CE1	√	√	√
	ID S1 CE2	√	√	*
	ID S2 CE1	√	√	√ / *
	ID S2 CE2	√	√	√ / *

GTX – geotextile | GGR - geogrid

UND - undamaged | ID - installation damage | S - soil | CE - compaction energy

√ - test performed | * - on-going tests

605

606 **Table 2 – Mean values of tensile tests results (5 specimens), with 95% confidence interval, for undamaged and damaged samples.**

Sample		T_{max} (kN/m)	ε_f (%)	$J_{2\%}$ (kN/m)	$J_{5\%}$ (kN/m)
GTX	UND	77.5 ± 1.7	13.0 ± 0.8	504.5 ± 97.3	657.2 ± 60.9
	ID S1 CE1	43.7 ± 4.7	8.8 ± 1.4	473.6 ± 33.8	605.3 ± 12.6
	ID S1 CE2	26.4 ± 1.6	7.1 ± 0.7	456.6 ± 48.9	476.0 ± 33.8
	ID S2 CE2	70.2 ± 0.9	11.7 ± 0.8	511.1 ± 60.9	642.7 ± 51.3
GGR	UND	83.4 ± 2.5	14.9 ± 1.1	680.4 ± 24.0	385.6 ± 19.6
	ID S1 CE1	52.0 ± 5.7	11.8 ± 0.7	645.4 ± 23.8	370.4 ± 10.3
	ID S1 CE2	45.9 ± 5.0	11.9 ± 0.4	480.4 ± 168.0	335.1 ± 38.3
	ID S2 CE1	64.5 ± 4.8	13.8 ± 0.8	594.0 ± 65.4	343.3 ± 29.9
	ID S2 CE2	62.2 ± 4.9	13.2 ± 0.5	587.2 ± 50.5	357.5 ± 21.3

GTX – geotextile | GGR – geogrid | UND – undamaged | ID - installation damage | S - soil | CE - compaction energy

607

608 **Table 3 – Reduction factors for installation damage and creep (extrapolations for a design time t_D=30 years) derived from the test results.**

Sample		RF_{ID} (T)	RF_{ID} (J2%)	RF_{ID} (J5%)	$RF_{CR\,(T)}$ (tD=30years)	$RF_{ID+CR\,(T)}$	$RF_{ID} \times RF_{CR}$ (T)	RF_{CR} (J2%)	RF_{CR} (J5%)	RF_{ID+CR} (J2%)	$RF_{ID} \times RF_{CR}$ (J2%)	RF_{ID+CR} (J5%)	$RF_{ID} \times RF_{CR}$ (J5%)
		[1]	[2]	[3]	[4]	[5]	[6]	[7]	[8]	[9]	[10]	[11]	[12]
GTX	UND	-	-	-	2.08	-	-	2.96	4.04	-	-	-	-
	ID S1 CE1	1.77	1.07	1.09	5.44	9.62	3.68	1.26	1.21	3.74	3.15	4.89	4.39
	ID S1 CE2	2.94	1.11	1.38	[b]	[b]	6.12	1.35	1.29	3.98	3.27	5.21	5.58
	ID S2 CE2	1.10	0.99[a]	1.02	2.66	2.94	2.29	1.15	1.09	3.39	2.92	4.39	4.14
GGR	UND	-	-	-	1.68	-	-	2.72 [b]	1.54	-	-	-	-
	ID S1 CE1	1.60	1.05	1.04	1.68	2.70	2.69	1.14 [b]	1.02	3.10	2.87	1.57	1.60
	ID S1 CE2	1.81	1.42	1.15	*	*	3.04	0.96[a,b]	1.23	2.62	3.86	1.89	1.77
	ID S2 CE1	1.29	1.15	1.12	1.66	2.14	2.17	1.08 [b]	1.05	2.94	3.12	1.62	1.72
	ID S2 CE2	1.34	1.16	1.08	1.63	2.32	2.25	1.1 [b]	1.12	3.16	3.16	1.72	1.66

GTX – geotextile | GGR – geogrid | UND – undamaged | ID - installation damage | S - soil | CE - compaction energy
* - not tested | [a] – below the minimum | [b] – value obtained with little meaning

609

610 # FIGURES

611

612 **Figure 1 – Geosynthetics tested: geotextile GTX and geogrid GGR.**

613

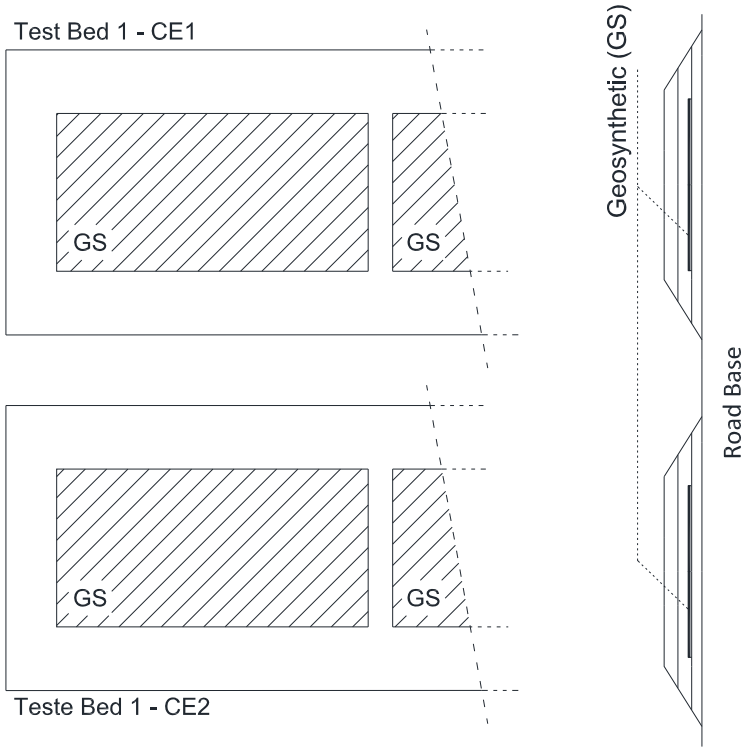

Figure 2 – Schematic representation of one set of test beds (one soil and two compaction energies): a) plan view; b) cross-section (not to scale).

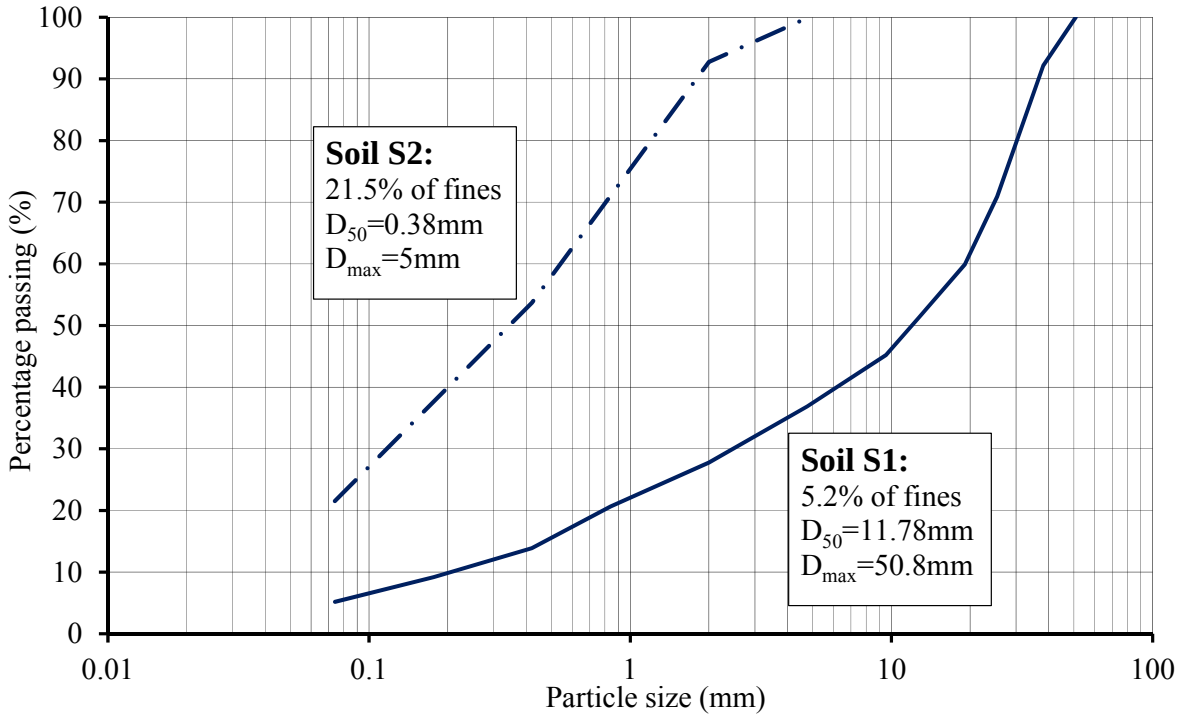

616

617 **Figure 3 – Particle size distribution of soils S1 (crushed aggregate) and S2 (residual soil from granite).**

618

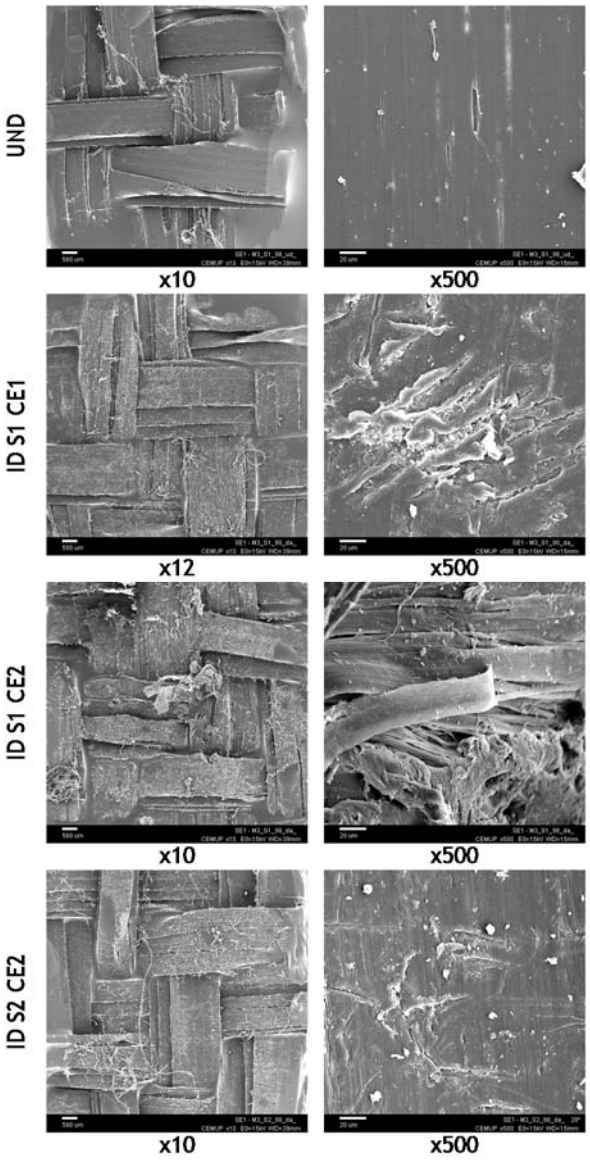

Figure 4 – Scanning electron microscopy images of geotextile GTX: undamaged (UND); exhumed from soil S1 poorly compacted (ID S1 CE1); exhumed from soil S1 well compacted (ID S1 CE2); exhumed from soil S2 well compacted (ID S2 CE2).

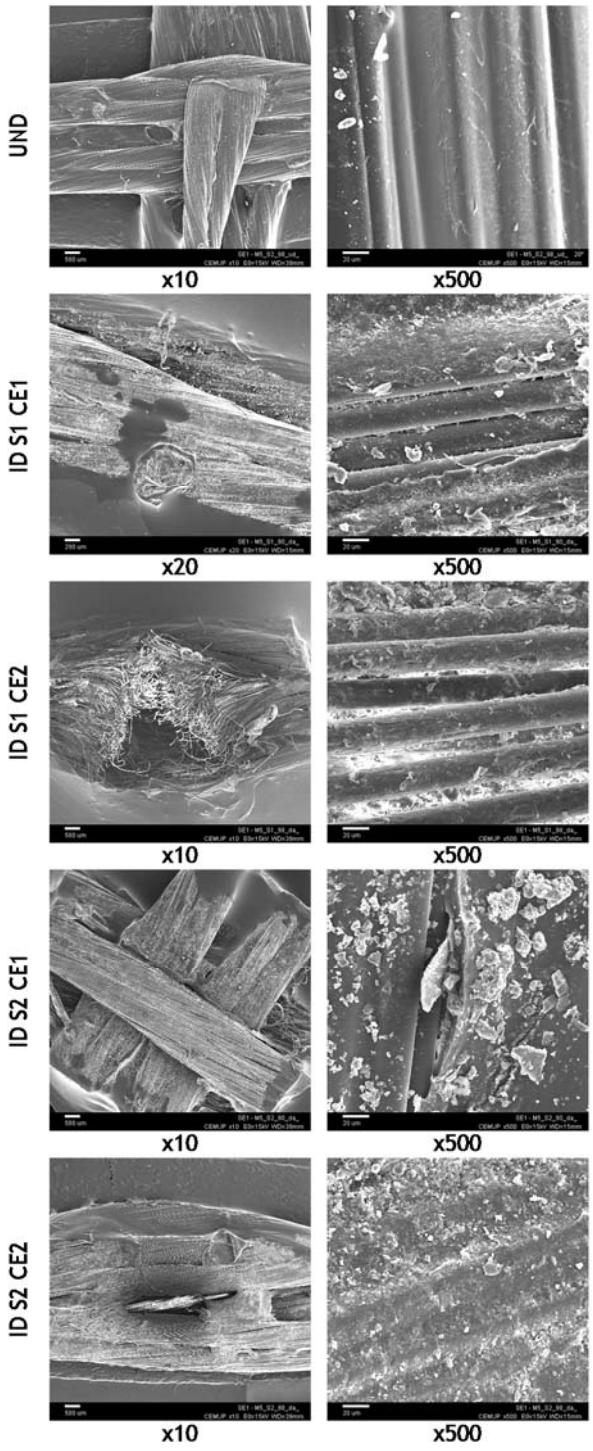

623

624 **Figure 5 – Scanning electron microscopy images of geotextile GGR: undamaged (UND); exhumed from soil**
625 **S1 poorly compacted (ID S1 CE1); exhumed from soil S1 well compacted (ID S1 CE2); exhumed from soil**
626 **S2 poorly compacted (ID S2 CE1); exhumed from soil S2 well compacted (ID S2 CE2).**

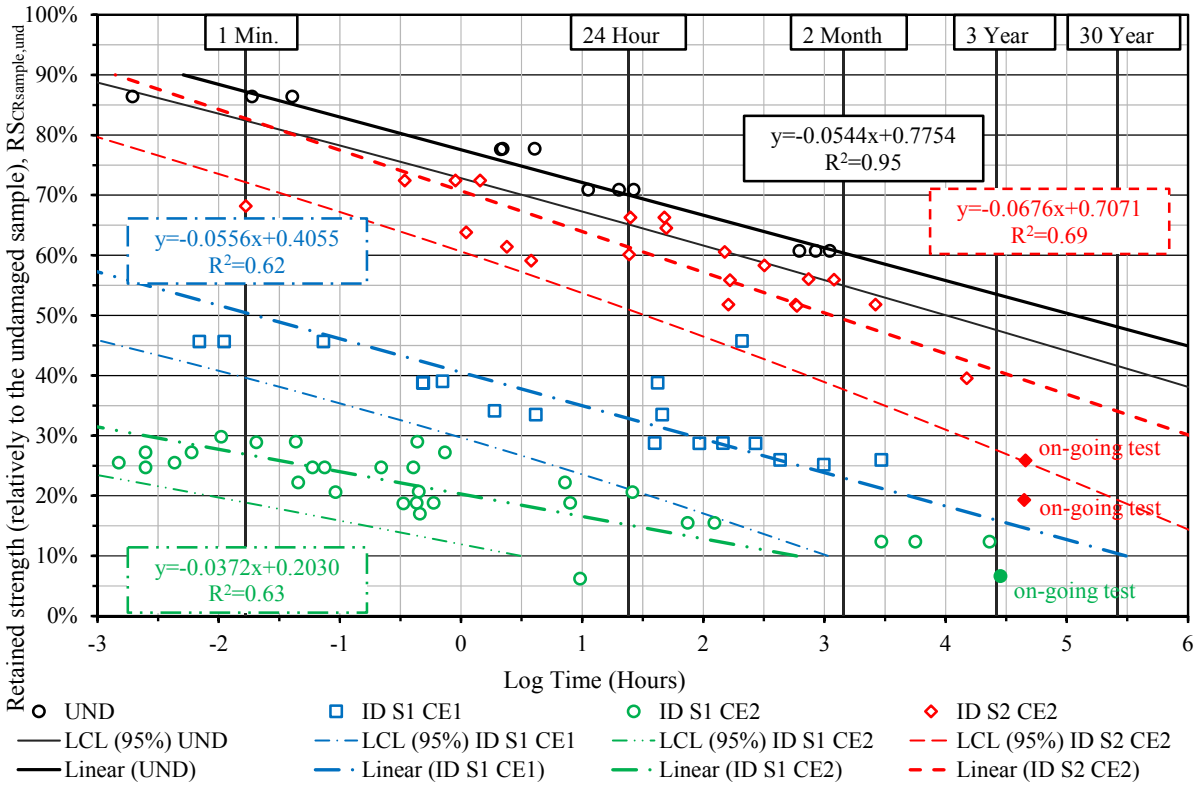

a)

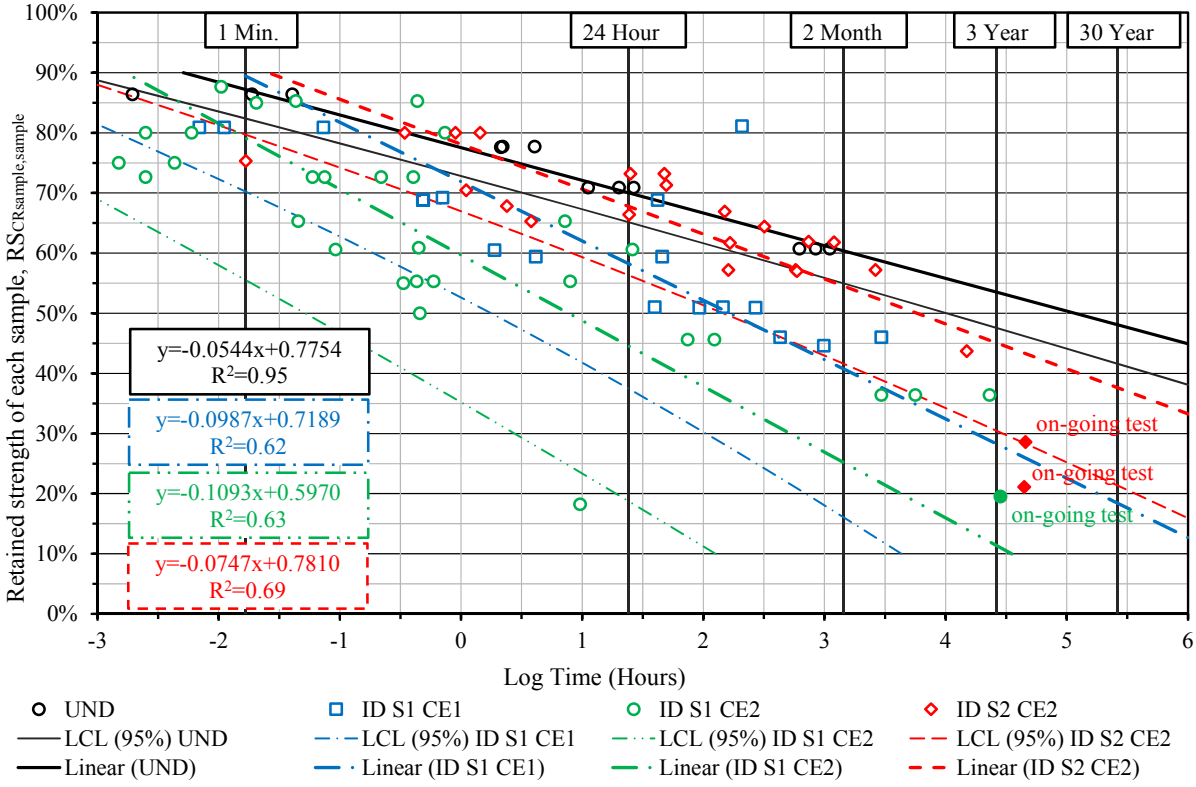

b)

Figure 6 – Creep rupture curves for GTX, undamaged and after field installation damage (S1 CE1, S1 CE2 and S2 CE2) as a function of: a) retained strength relatively to the undamaged material ($RS_{CRsample,und}$) versus time to rupture; b) retained strength of each sample ($RS_{CRsample,sample}$) versus time to rupture).

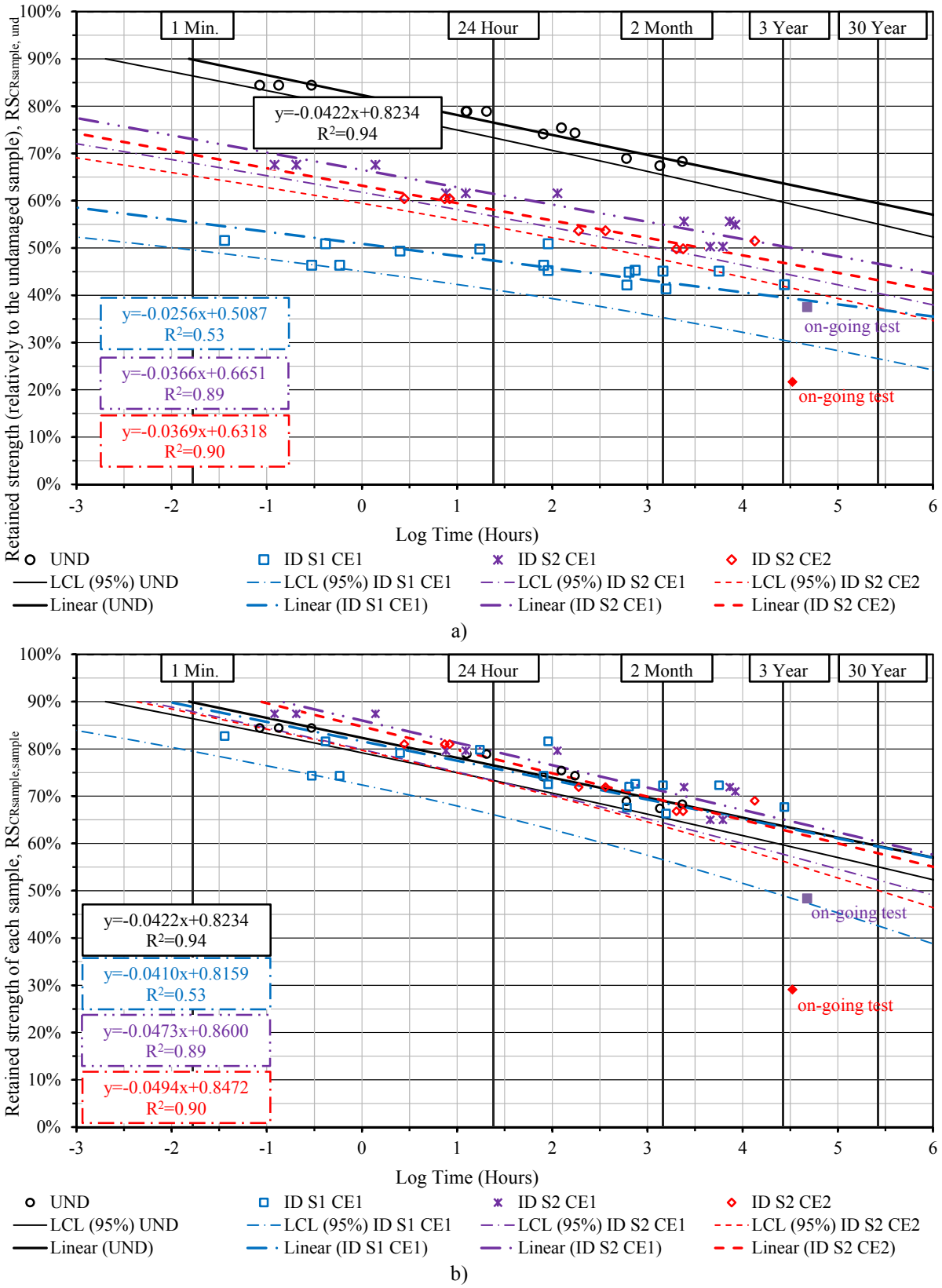

Figure 7 – Creep rupture curves for GGR, undamaged and after field installation damage (S1 CE1, S2 CE1 and S2 CE2) as a function of: a) retained strength relatively to the undamaged material ($RS_{CRsample,und}$) versus time to rupture; b) retained strength of each sample ($RS_{CRsample,sample}$) versus time to rupture).

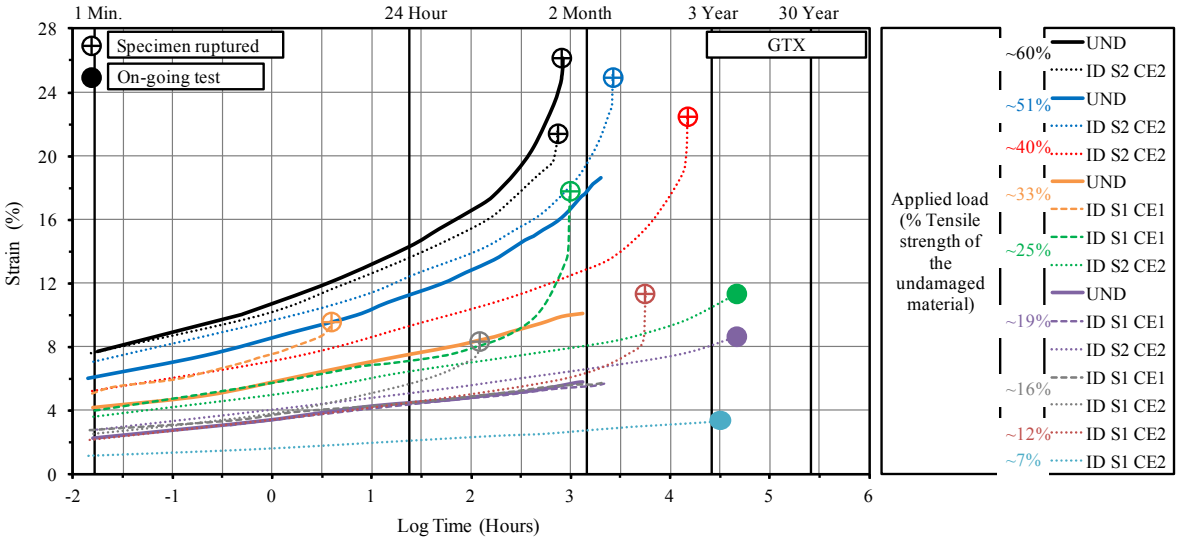

a)

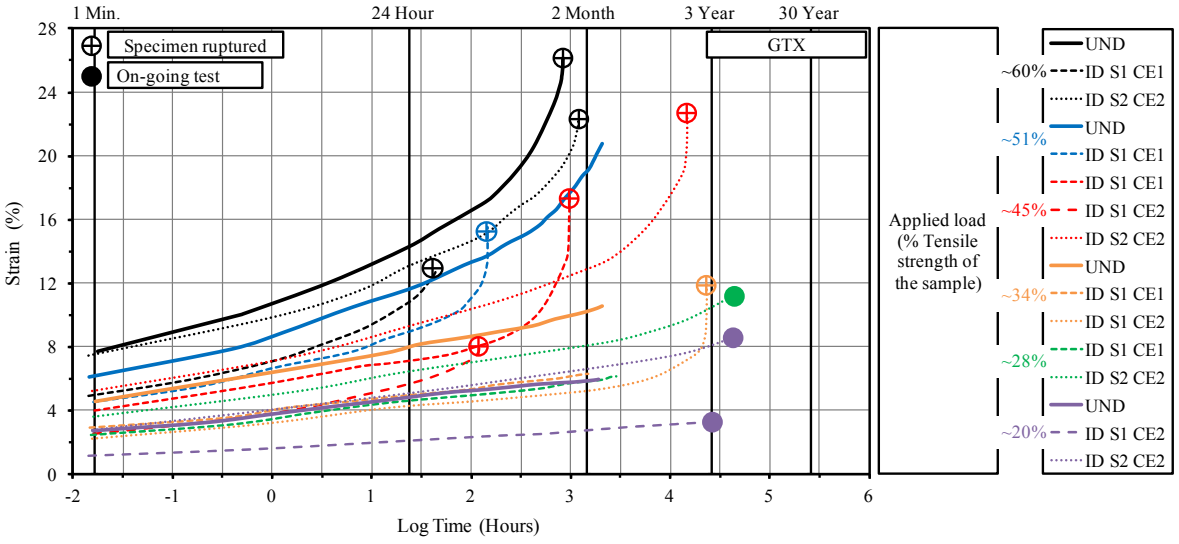

b)

Figure 8 – Creep curves for GTX, undamaged and after field installation damage (S1 CE1, S1 CE2 and S2 CE2): a) applied load represented relatively to the tensile strength of the undamaged material; b) applied load represented relatively to the tensile strength of each sample. [Data for different specimens are included in the two parts of the figure]

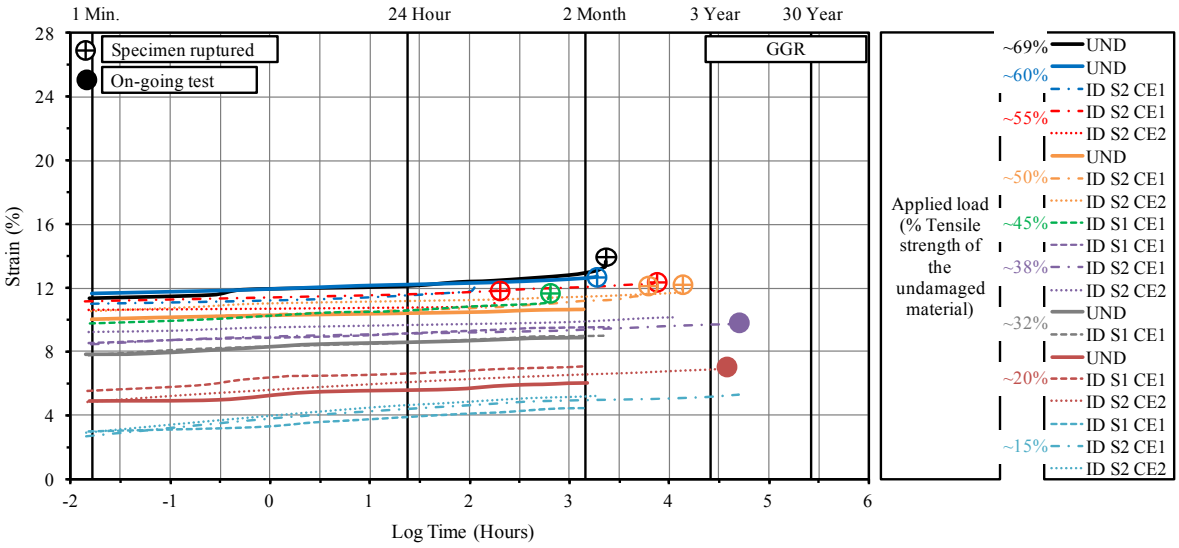

a)

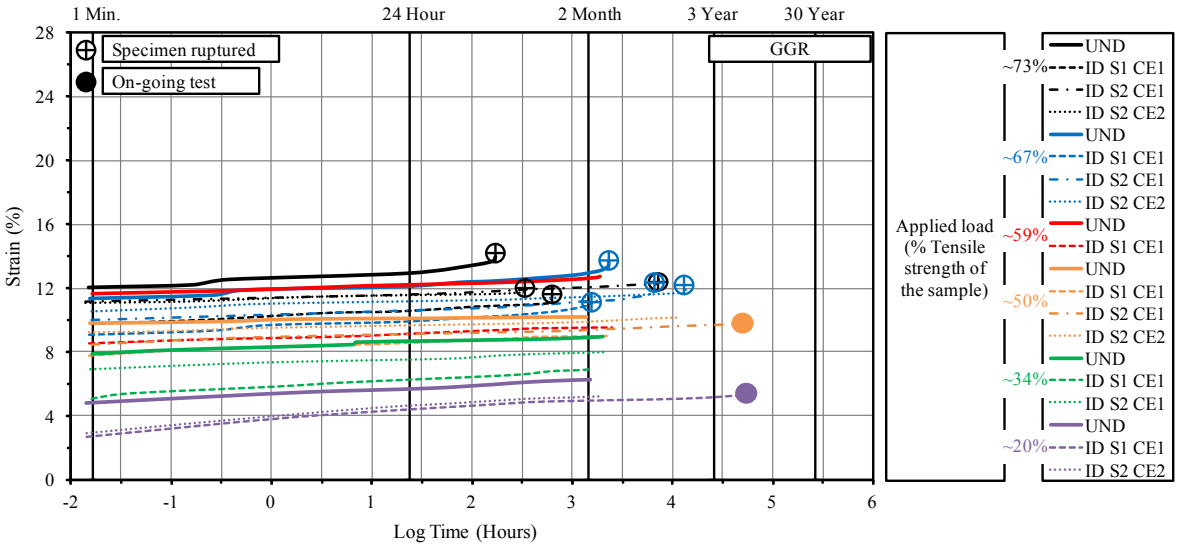

b)

Figure 9 – Creep curves for GGR, undamaged and after field installation damage (S1 CE1, S2 CE1 and S2 CE2): a) applied load represented relatively to the tensile strength of the undamaged material; b) applied load represented relatively to the tensile strength of each sample. [Data for different specimens are included in the two parts of the figure].

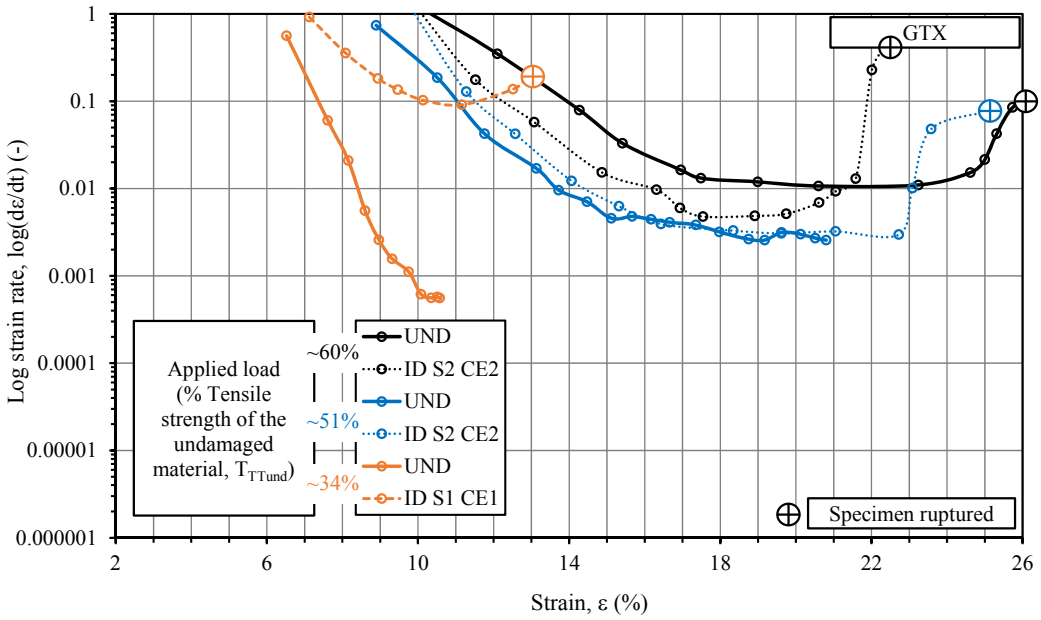

a)

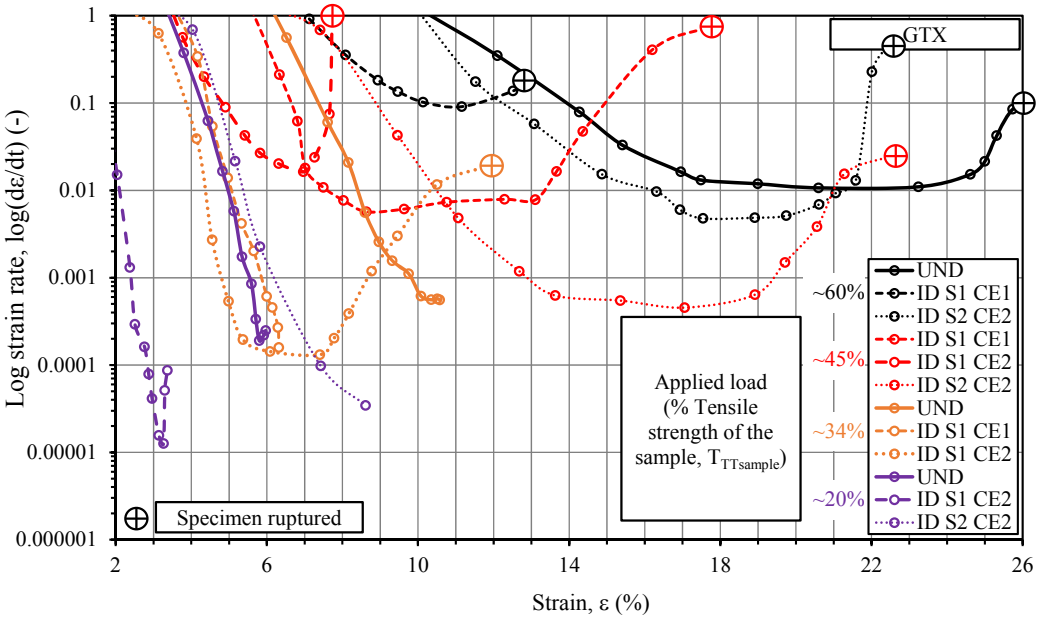

b)

Figure 10 – Sherby-Dorn plots (strain rate – strain) and derivate of Sherby-Dorn – strain for GTX, undamaged and after field installation damage (S1 CE1, S1 CE2 and S2 CE2) for specimens tested under the same load relatively to: a) the undamaged sample; b) the tensile strength of each sample [Data for different specimens are included in the two parts of the figure].

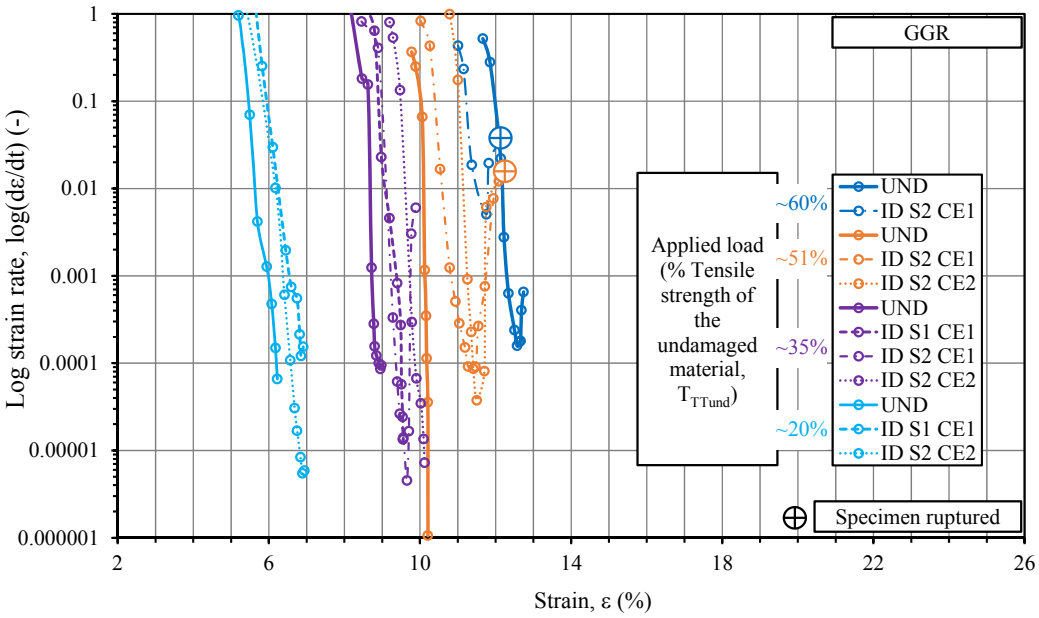

a)

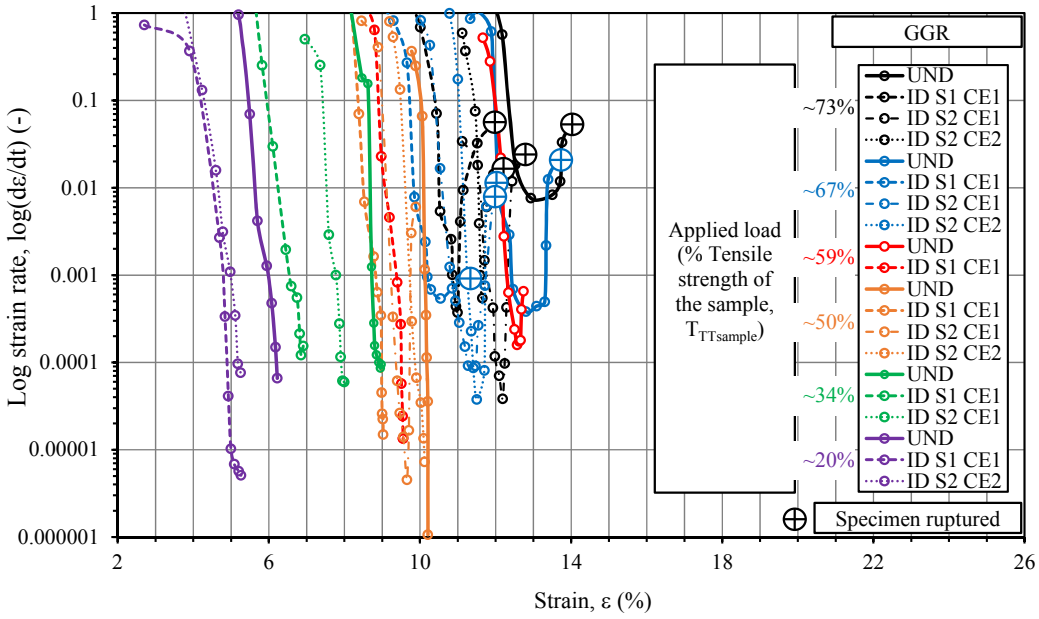

b)

Figure 11 – Sherby-Dorn plots (strain rate – strain) and derivate of Sherby-Dorn – strain for GGR, undamaged and after field installation damage (S1 CE1, S2 CE1 and S2 CE2) for specimens tested under the same load relatively to: a) the undamaged sample; b) the tensile strength of each sample [Data for different specimens are included in the two parts of the figure].

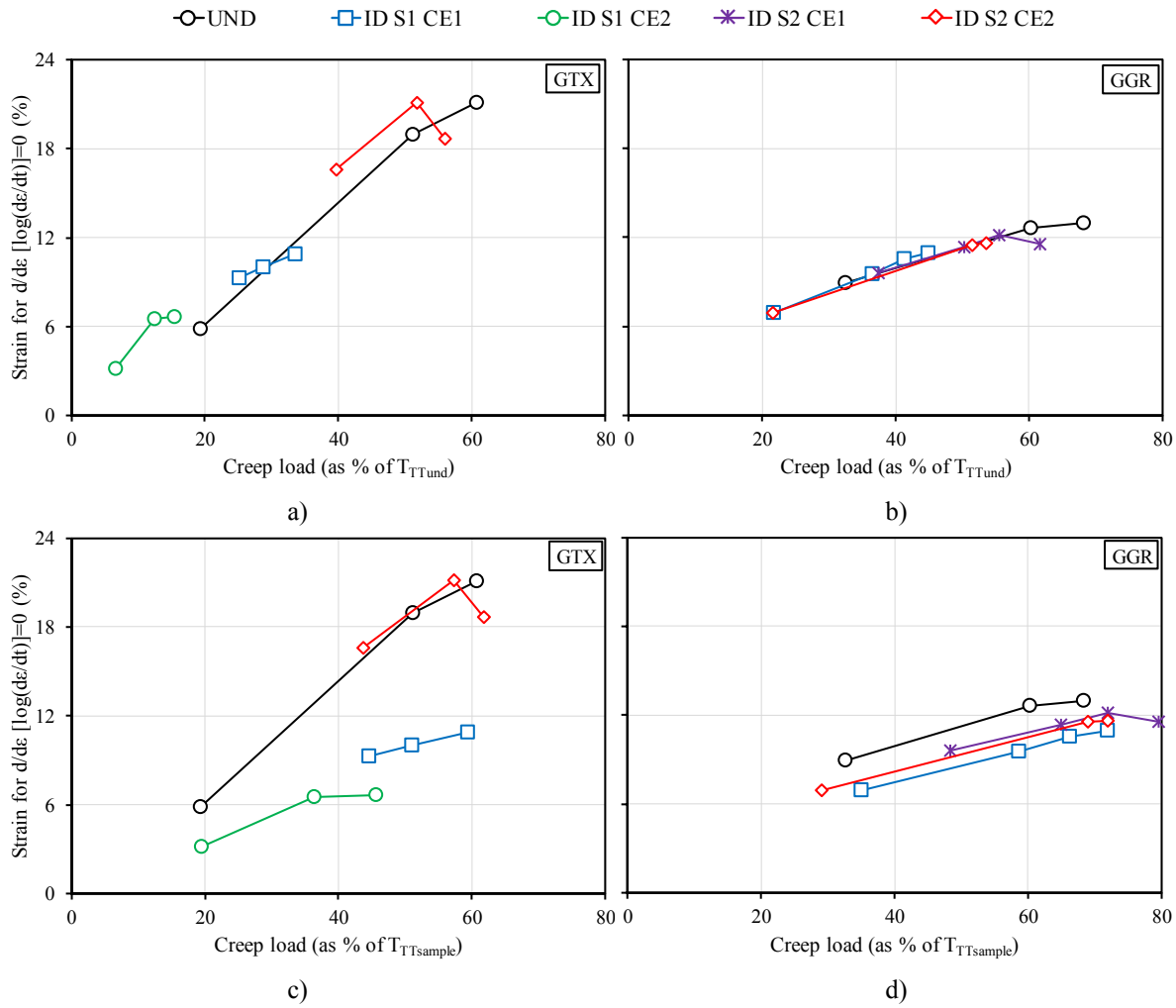

649 **Figure 12 – Strain for $\frac{d}{d\varepsilon}\left[\log\left(\frac{d\varepsilon}{dt}\right)\right] = 0$ for specimens of GTX and GGR undamaged and after field**
650 **installation damage tested under the same creep load relatively to the undamaged sample a) GTX; b) GGR**
651 **and to the tensile strength of each sample c) GTX d) GGR.**

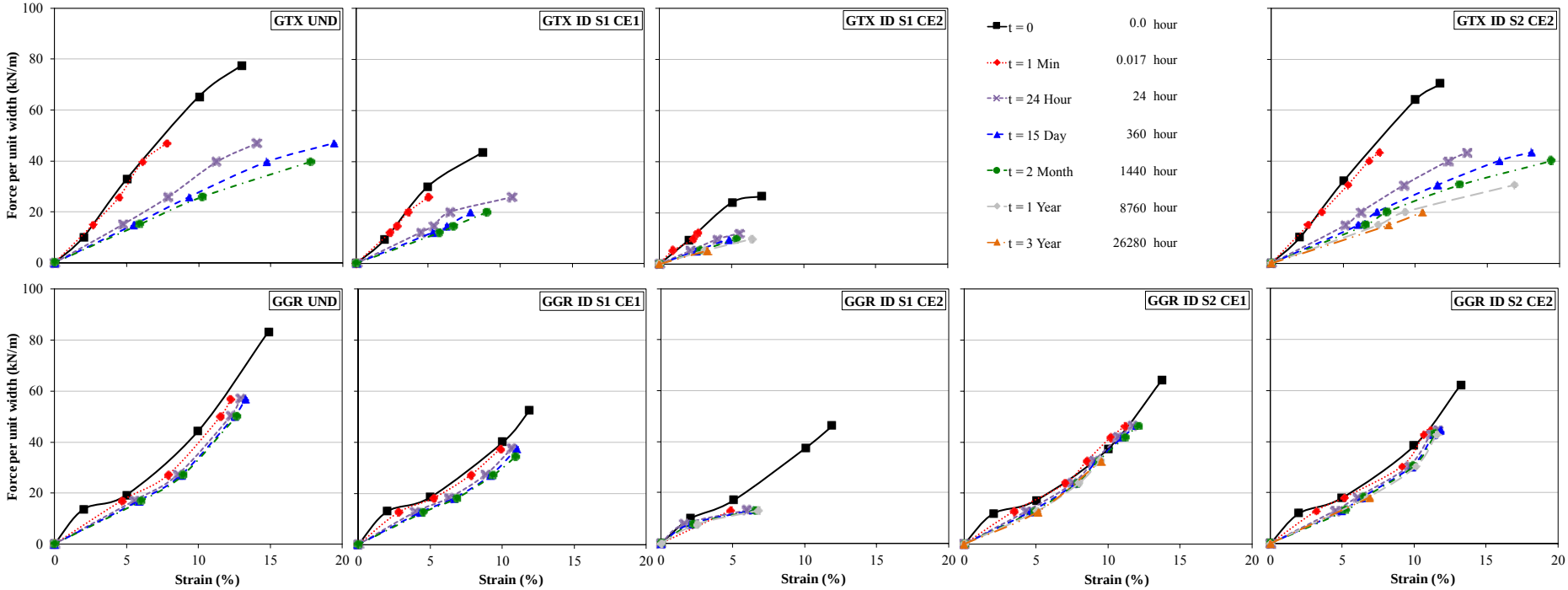

Figure 13 – Isochronous curves for GTX, undamaged and after field installation damage (S1 CE1, S1 CE2 and S2 CE2) and GGR, undamaged and after field installation damage (S1 CE1, S1 CE2, S2 CE1 and S2 CE2).

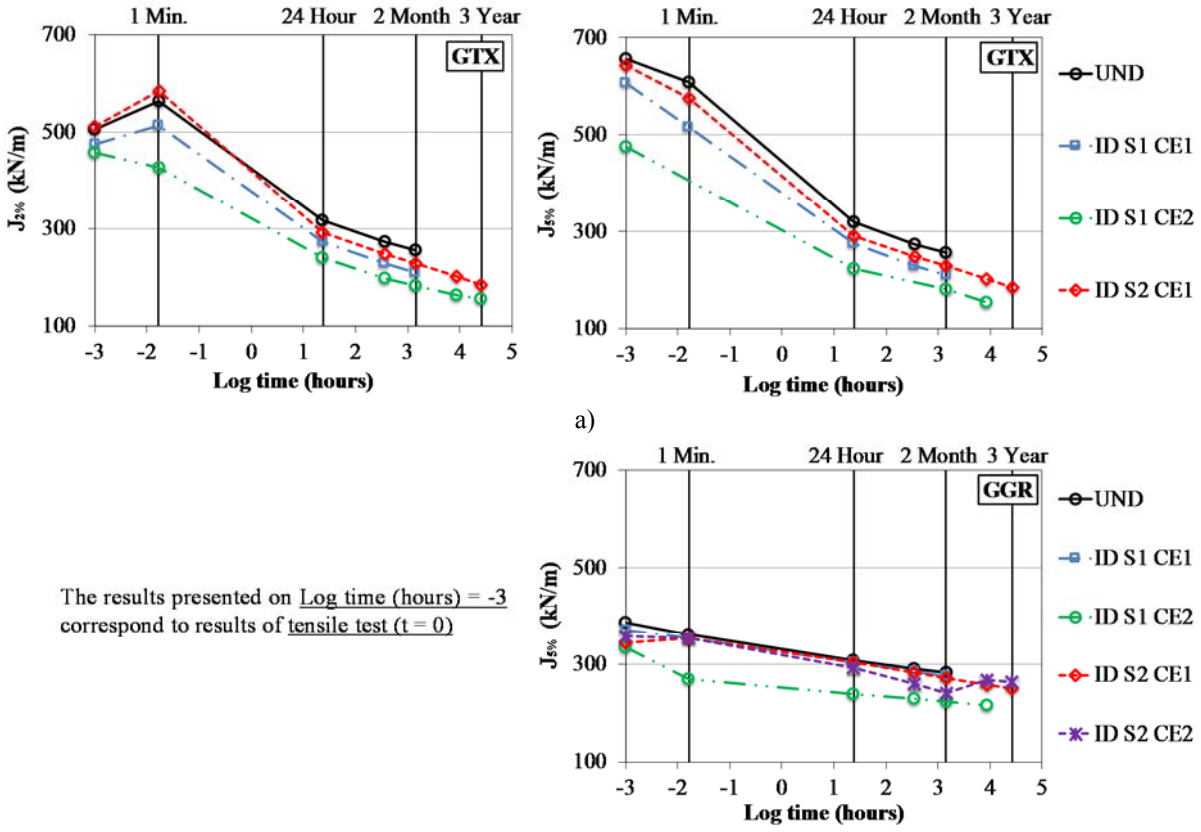

Figure 14 – Secant stiffness modulus $J_{2\%}$ and $J_{5\%}$ versus time: a) GTX, undamaged and after field installation damage (S1 CE1, S1 CE2 and S2 CE2); b) GGR, undamaged and after field installation damage (S1 CE1, S1 CE2, S2 CE1 and S2 CE2).

SUPPLEMENTARY FIGURES

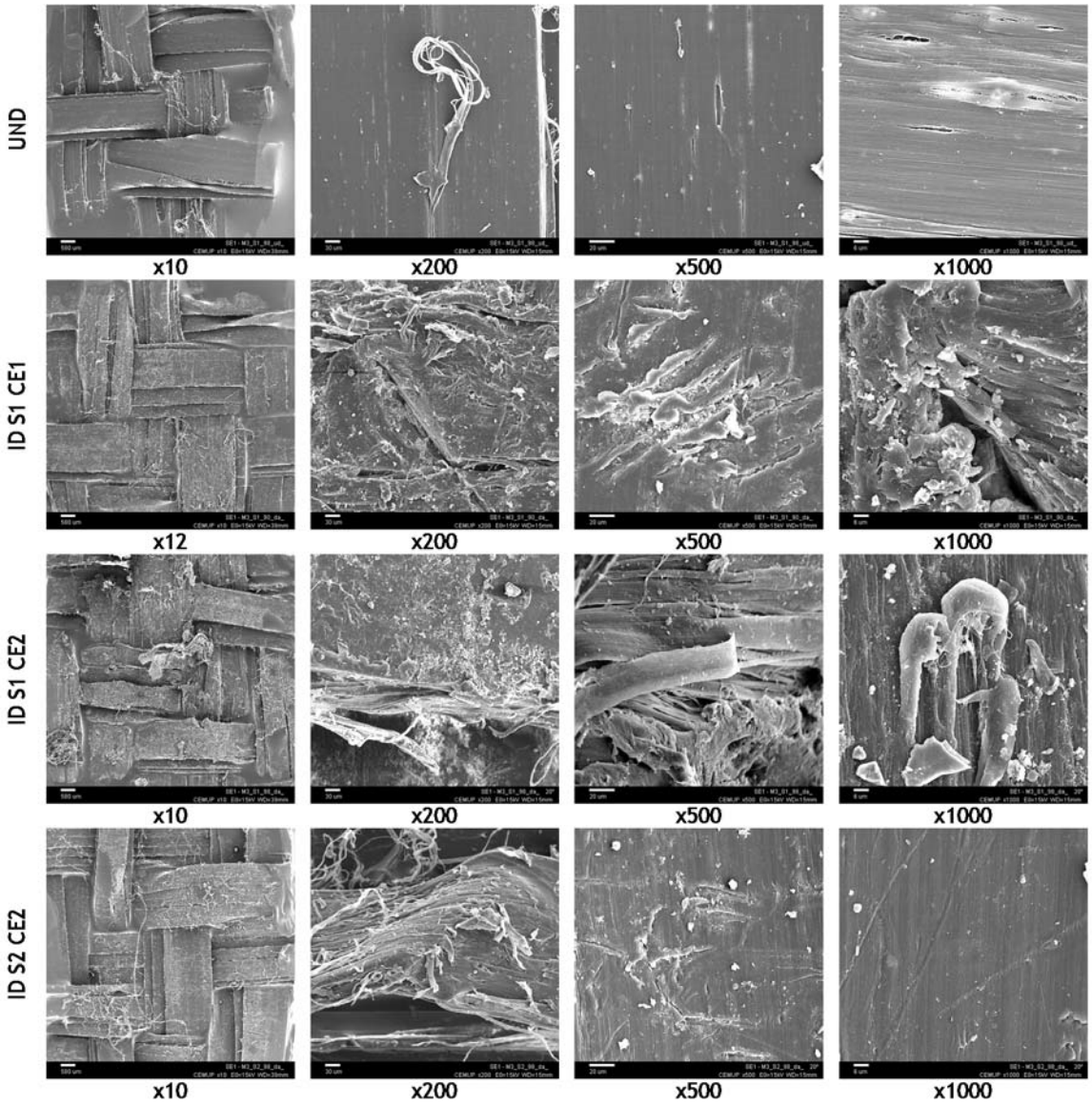

Figure Sup. 1 – Scanning electron microscopy images of geotextile GTX: undamaged (UND); exhumed from soil S1 poorly compacted (ID S1 CE1); exhumed from soil S1 well compacted (ID S1 CE2); exhumed from soil S2 well compacted (ID S2 CE2).

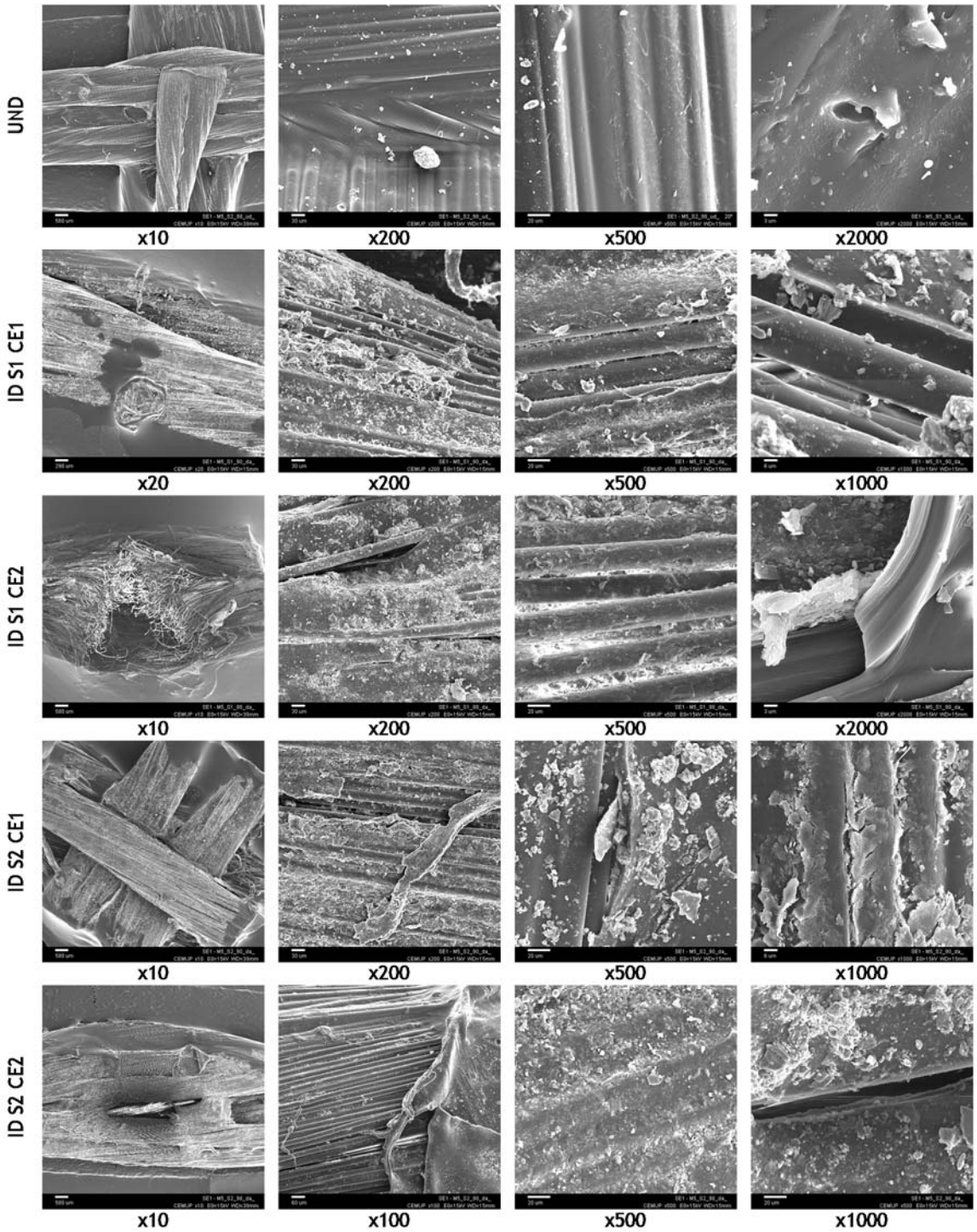

Figure Sup. 2 – Scanning electron microscopy images of geotextile GGR: undamaged (UND); exhumed from soil S1 poorly compacted (ID S1 CE1); exhumed from soil S1 well compacted (ID S1 CE2); exhumed from soil S2 poorly compacted (ID S2 CE1); exhumed from soil S2 well compacted (ID S2 CE2).